International Journal of Engineering Research and Development
e- ISSN: 2278-067X, p-ISSN: 2278-800X, www.ijerd.com
Volume 22, Issue 2 (February 2026), PP 240-283

Rotor Angle Stability Analysis of a Power System with Renewable Energy (Photovoltaic System) Integration

Williams Adegoke Malik[1], Sabo Aliyu[1], Dauda Dahiru[1*]
[1,,2,3]*Department of Electrical/Electronic Engineering, Faculty of Engineering and Engineering Technology, Nigerian Defence Academy, Kaduna.*

Abstract
A single-machine infinite bus (SMIB) model was modelled in MATLAB Simulink environment to study rotor angle stability. A three-phase balanced fault is then caused on the SMIB system to simulate a large disturbance. The SMIB generator rotor speed deviation response reaches a settling time of 3.1 seconds (out of 10 seconds simulation time). A Power System Stabilizer (PSS) damping controller is designed and optimized using the Transit Search Optimization algorithm (TS) to obtain optimised parameters KG, T1, T2, T3, T4 to enable the control of the generator rotor speed deviation at 1.5 seconds settling time. The proposed controller was validated by comparing it to genetic algorithm optimized PSS at 1.9 seconds settling time and particle swarm optimized PSS at 1.89seconds settling time. Furthermore, a solar photovoltaic (PV) generator was integrated into the SMIB system and the Transit Search optimised PSS damping controller was able to control the generator rotor speed deviation at 3.0 seconds settling time. The results showed that the proposed Transit search optimized PSS damping controller can control electromechanical oscillations in a single-machine infinite bus system and also in an integrated single-machine infinite bus and solar integrated generator (PV) system which leads to improved rotor angle stability.

Date of Submission: 14-02-2026 Date of acceptance: 28-02-2026

I. Background of the Study

Electrical power is directly in variance with the economic development of any nation and its importance can no longer be over emphasised. Hence, we can reach a logical conclusion that the GDP of a Country is proportional to the quantum of electric power available to drive industrialisation and human resource development. Therefore, the reliability, security and stability of the power system is critical for the daily living of the human race.

The Power System is a nonlinear and complex system which involves the conveyance of bulk power from generating stations through transmission lines to bulk load centres where the power is distributed by MV distribution lines as shown in Figure 1. This makes the power grid one of the largest single networks on planet earth.

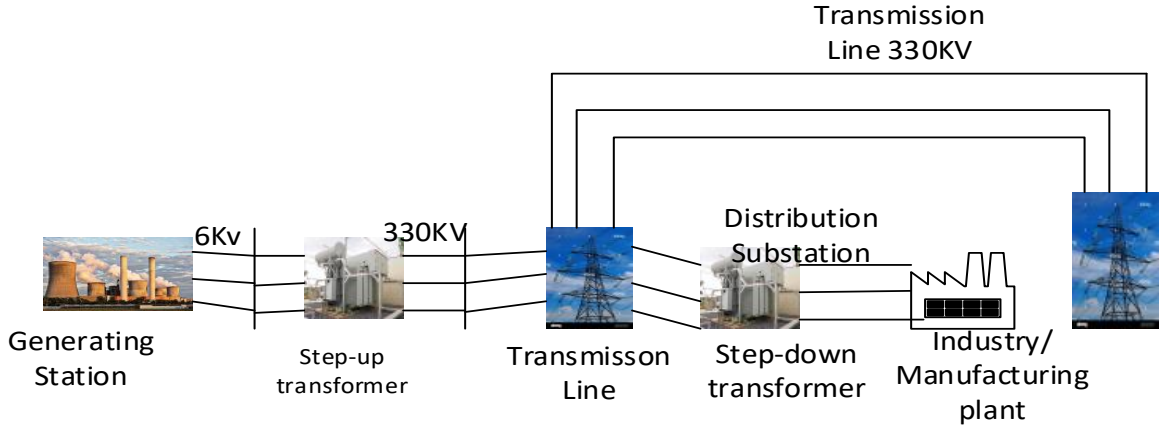

Figure 1: Typical Power System showing Generation, Transmission and Distribution

The worldwide demand for energy, particularly cleaner and environmentally friendly electric energy is continually expanding in tandem with time. Although, fossil fuel-based energy sources are still abundantly available, global concerns pertaining to climate change has led to the increase in demand for renewable energy sources. This trend has propelled advancement in renewable energy technology such as Wind and Solar (PV). The

integration of renewable energy sources (RES) into the conventional grid, which is essentially made up of synchronous generators has brought about varying questions with respect to low frequency oscillations as to rotor angle stability, voltage fluctuations as to voltage stability, frequency stability, load dispatch, spinning reserve among others. This thesis will be focusing on the analysis of low frequency oscillations as a result of the integration of Solar (PV) into the conventional grid.

These oscillations are frequencies of electromechanical modes within the power system and may be local or interarea. Research made by [1] and [2] highlighted some of the challenges of integration of renewable energy into the grid inclusive of low frequency oscillation. These uncontrolled oscillations will have a negative impact on the power system and disrupt the smooth operation of the grid as recorded during blackouts which occurred in various parts of the world [3].

Because of inadequate damping of the low frequency electromechanical oscillation modes, this results in loss of synchronism of the power system and eventual black out. Hence, damping controllers play a key role in the dynamic stability of a power system and addressing low frequency oscillations is a global concern.

The Power System Stabilizer (PSS) is a primary damping scheme and is traditionally connected to the exciter and located in the synchronous generator to damp electromechanical oscillations and enhance the stability of the power system. The PSS always produces positive damping while the Automatic Voltage Regulator produces negative damping and synchronising torque to the system[4]. The goal of this stabilizer is to restore the rotor speed of the generators to their rated value. Utilizing the PSS has proven to be effective when the parameters are designed utilizing an effective optimization technique[5]. Fixed parameters of the conventional PSS cannot handle the wide operating range of the oscillations. Therefore, the robust design of controllers is an optimisation problem and the only possible solution against oscillations in power systems to ensure safe operation of damping controllers. Time domain simulations and convergence analysis are also conducted to understand how the power system responds to small signals.

Among the list of renewable energy sources, reviews have shown that wind and solar will dominate renewable energy sources that will be integrated into the grid. There are two distinct methods of solar power generation, solar photovoltaic and concentrated solar thermal. Out of this two, solar photovoltaic is more financially viable and matured. Concentrated solar plants are capital intensive and require very high intensity of solar irradiation to meet the thermal requirements for generating electricity[6]. It is getting more popular in countries like the USA, China and Germany to have solar farms with numerous solar panels covering large expanse of land and even water body feeding through converter generators to the grid. Due to this integration and the resultant impact, the Western Electricity Coordinating Council (WECC) developed models that may be employed for analysis basis.

Due to the injection of power from (Solar PV) electronic generators at transmission levels or higher voltages into the conventional grid, there is the need to analyse the dynamics of the rotor angle of the synchronous generator with renewable penetration (Solar PV) in the event of a fault. This research aims to study the **rotor angle stability analysis of a power system with renewable energy (Photovoltaic System) integration**. This aim will be achieved through the following objectives:

i. Model a Single Machine Infinite Bus (SMIB) Test System and a Grid-Connected Photovoltaic System in a SIMULINK environment.
ii. Introduce a fault on the SMIB system to observe the rotor angle stability. Introduce a power system stabiliser (PSS) as a damping controller with parameters optimised with the Transit Search Algorithm, Particle Swarm Optimisation (PSO) and the Genetic Algorithm (GA) and compare the performance of the TS-PSS with that of the Particle Swarm Optimisation algorithm (PSO-PSS) and Genetic Algorithm (GA -PSS) with the aim of analysing the rotor angle stability when damping low frequency oscillations.
iii. Integrate the Photovoltaic System with the SMIB power system and analyse the stability of the rotor angle at the event of a fault then introduce the Transit Search optimised damping controller (TS-PSS) to analy the rotor angle stability.

The scope of this research will be to conduct Non -Linear Time Domain Simulations to obtain rotor speed deviations. Under different loading conditions, an exhaustive small signal stability study will be conducted on the SMIB test system and will be presented under the following scenarios:

Case 1: Simulate the SMIB system with no renewable penetration and PSS
Case 2: Simulate the SMIB system with PSS
Case 3: Simulate the SMIB system with renewable penetration and PSS

1.2 Significance of the study

The significance of this study is highlighted below:

i. The study will avail the opportunity to analyse the behaviour of the power system rotor angle, using the SMIB as the test model, under the integration with renewable energy source such as the Solar (PV).

ii. The study will give an opportunity to apply artificial intelligence methods such as the Transit Search optimisation algorithm and other established metaheuristic algorithms to optimise damping controller parameters inorder to dampen low frequency oscillations in the power system.

iii. The design will be essential for power system designers, planners, government and regulatory bodies, synchronous generator designers, students and researchers towards understanding the PSS and power system stability as a whole.

iv. This research will also contribute and allay the fears in the field of renewable energy and its integration to the grid with respect to power system stability.

2.1 Power system stability and Low Frequency oscillations

Understanding power system stability and the causes of instability requires that we understand the different forms of stability and their classifications in the power system. The analysis of stability including identifying key factors that contribute to instability and devising methods of improving stable operation, is greatly facilitated by classification of stability into appropriate categories[9]. Figure 2.1 shows the classification of power system stability. This study is mainly concerned with rotor angle stability and its related issues.

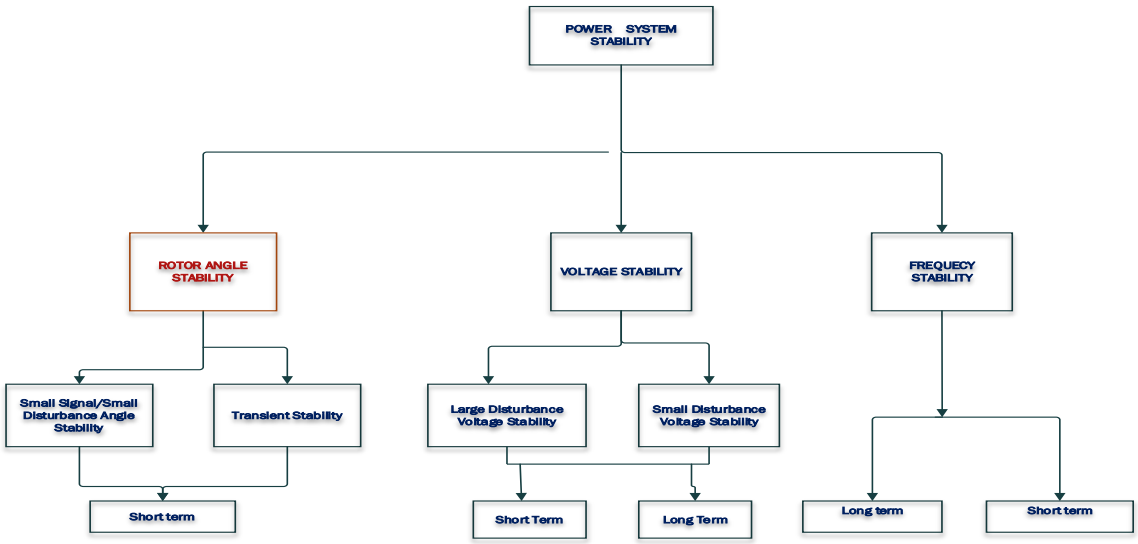

Figure 2.1 *Classification of power system stability[9]*

2.1.2 Rotor Angle Stability

Rotor angle stability refers to the ability of synchronous machines of an interconnected power system to remain in synchronism after being subjected to a disturbance[8]. It depends on the ability to maintain/restore equilibrium between electromagnetic torque and mechanical torque of each synchronous machine in the system. The rotor angle stability problem involves the study of the electromechanical oscillations inherent in power system[7].

Fundamentally, there is a relationship between the output power of the generators and the rotor angle, so for every change in power there is a resultant change in rotor angle. Under steady state, there is an equilibrium set between the power output, rotor angle and speed of the generator. Take for instance (n) number generators running synchronously, suddenly there is a perturbation and one or more generators is lost due to this action, at this stage, one would expect a resultant deceleration or acceleration of the other generators and also an upset of the rotor angle according to the laws of motion of a rotating body. If one generator begins to run faster or slower than the other generator, the angular position of the rotor angle begins to shift higher or lower relative to the other generator. Consequently, the resulting angular difference transfers part of the load from the slower generator to the faster generator depending on the power angle relationship. For any given situation, the stability of the system depends on whether or not the deviations in angular positions of the rotors result in sufficient restoring torques. The swing equation best describes this relationship. The chain of this event leads to the build-up of oscillations in power system. Figure 2.2 shows an illustration of the relationship between the power output, speed and rotor angle.

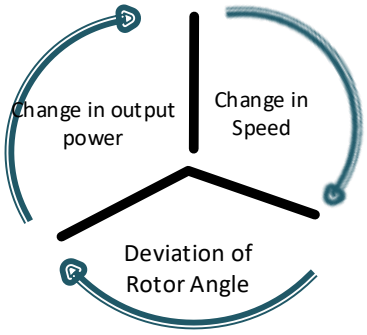

Figure 2.2 *Sequential events of electromechanical oscillations*

Small-disturbance rotor angle stability problems maybe either local, interarea or global in nature. Local problems involve a small part of the power system, and are usually associated with rotor angle oscillations of a single power plant against the rest of the power system. Interarea problems occur coherently between generators in different areas connected via tie lines while global problems are caused by interactions between large groups of generators and have widespread effects[4]. [10] in his study stated that these oscillations have low frequencies and can be classified into two main categories: local (typically 0.7–2 Hz) and interarea (0.1–0.7 Hz). The low frequency electromechanical oscillations, with frequency ranging from 0.1-2Hz, are inherent to electric power systems. The low frequency oscillations are related to the small signal stability of the power system and are detrimental to the goals of maximum power transfer and power system stability.

2.2 Single machine Infinite Bus

According to studies in [11], the simplest model to represent the synchronous machine is the classical model where saliency is ignored and commonly represented as an infinite bus with constant voltage (magnitude and angle) and frequency. It assumed to be infinite bus because its characteristics do not change irrespective of the power applied or consumed by a machine connected to it. The cylindrical rotor machine is modelled with a constant voltage source behind proper reactance which may be X''_d, X'_d or X_d which are the subtransient, transient and steady state reactances. Figure 2.3 depicts the single line diagram of the SMIB which has only one generator has the name implies.

To enable model the SMIB, the synchronous machine is represented as a group of magnetically coupled circuits with inductances which depend on the angular position of the rotor axis. The transformation of the stator variables is carried out using the two-axis theory. The reference frame theory is then used to transform the stator variables transformed into a fixed reference frame fixed in the rotor. Basically, there are two frames, the d and q reference frame.

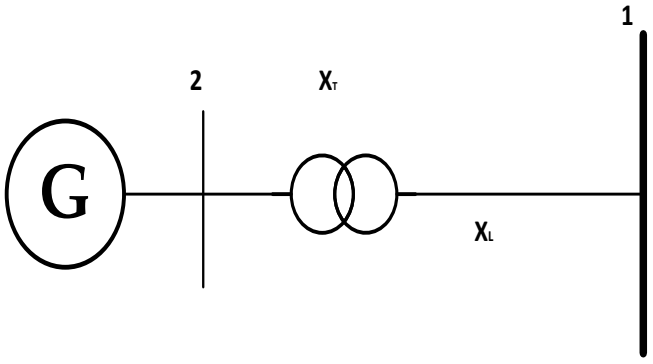

Figure 2.3 *Single Line model of the SMIB*

2.3 Solar (PV) Energy Conversion

There are two distinct methods of solar power generation, solar photovoltaic and concentrated solar thermal. Out of this two, solar photovoltaic is more financially viable and matured. Concentrated solar plants are capital intensive and require very high intensity of solar irradiation to meet the thermal requirements for generating electricity[6]. Solar Photovoltaic plants, henceforth referred to as PV, generate electricity from solar panels and have no need for rotating machines. The attractive features of the PV plant are its modularity, low maintenance and operations cost and environmental friendliness. The applications of Solar PV can be classified into four main

categories namely, off-grid domestic, off-grid non-domestic, grid-connected distributed and grid connected centralised[12].

For the sake of this study, grid connected distributed will be discussed. In other words, the grid centralised PV is a utility scale PV plant with voltages above 11KV depending upon the grid connection point and voltages and it provides bulk energy generated into the grid. Historically, PV installations have been small and distributed. As at 2009, majority of PV plants were connected at distribution levels, either on the secondary side of the local distribution transformers or primary distribution systems. However, after the installation of first ever transmission level (230 kV) utility-scale PV plant in USA (Desoto Solar Energy Centre in Florida), the interest in large-scale PV in transmission and sub-transmission systems has continued to grow. It is anticipated that Utilities will begin to face some new non-traditional operational problems due to the distinctly different in dynamic characteristics of large-scale PV compared to the conventional generators and its counterpart wind power.

Numerous PV generator models have been developed and reported in literatures however, there is no "industry standard model" for PV generator. Moreover, most of the developed PV generator models are suitable for power quality studies in distribution systems which includes detailed modelling of electro-magnetic transient behaviour of PV systems. The detailed PV modelling for fast transient studies is not necessarily required for the system wide stability impact studies where the focus is on electromechanical behaviour of the system. Therefore, the model to be adopted is the WECC model which is simple and appropriate for transmission and sub-transmission level stability studies. Details regarding the modelling of the solar PV can be found in [13]. The Western Electricity Coordinating Council (WECC) overall model for a large solar PV block diagram is placed in Figure 2.4. The dynamic representation uses three renewable modules. These modules are also used to represent wind and inverter-based energy storage systems. It includes, REGC: Renewable Energy Generator Converter Module. REEC: Renewable Energy Electrical Control Module and REPC: Renewable Energy Plant Control Module. Technical specifications for the Generic models are including in the WECC Solar Photovoltaic Power Plant Modelling Guideline[14].In this thesis, the distribution level solar pv system which is the model in Figure 2.4 but without the REPC, plant level controller. The WECC model also does not include solar irradiation block. This is represented by a constant block which receives frequency and voltage reference from a nearby synchronous generator.

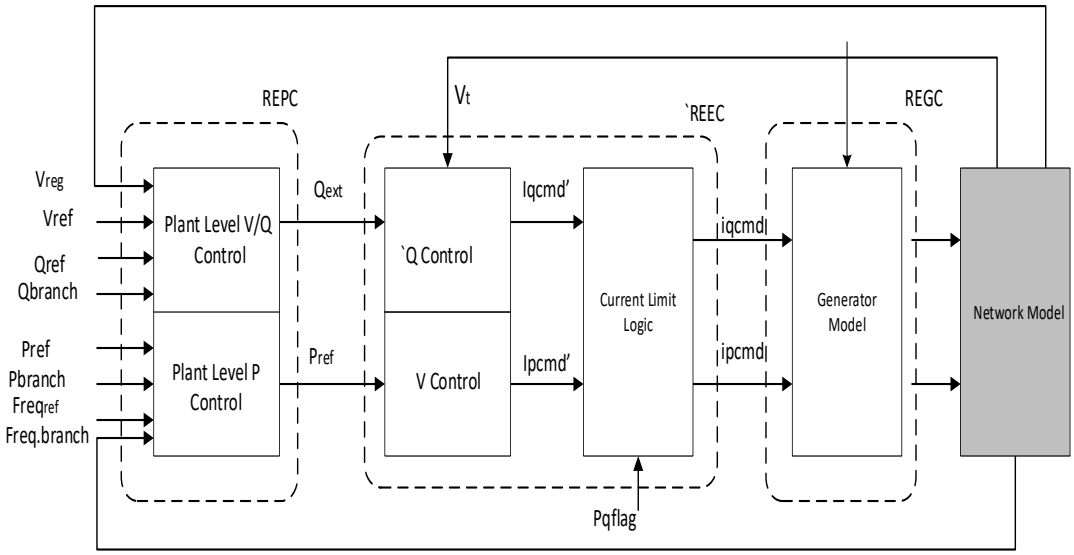

Figure 2.4 *WECC Generic PV Model[14]*

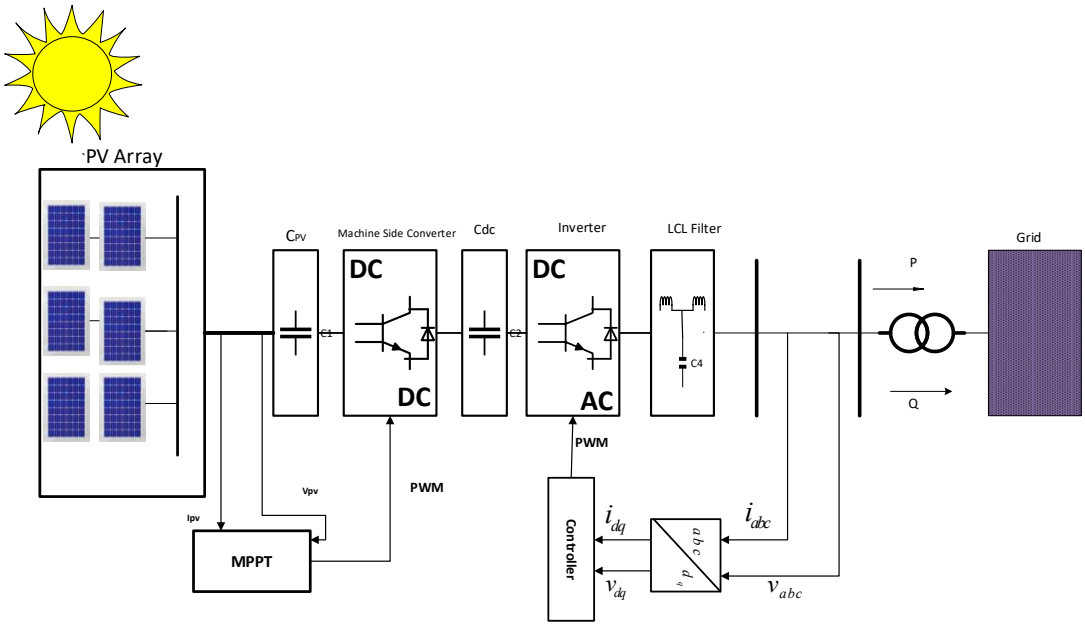

Figure 2.5 *Schematic Model of a Grid Connected PV System[13]*

2.4 Power System Stabiliser damping controller

The Power system stabiliser is traditionally used to damp out low frequency oscillations. The PSS came into existence between the 1950 – 1960's when the number of generators added to the utility increased due to increase in loads. PSS is a cost-effective technology which provides sufficient damping torque to the system[9]. The PSS always produces positive damping while AVR provides negative damping and synchronizing torque to the system. The modern stabilizers used in the market are of combinations of multi-band stabilizers. The multiband stabilizers are used to handle different oscillation frequencies and it has three separate signal bands. The Conventional PSS is a single band PSS which maybe analog or digital. It helps to maintain the small signal and transient stability. The conventional PSS has gain, washout filter and lead lag compensator. The conventional PSS performance is limited to wide area operating conditions. Figure 2.6 shows the structure of the conventional PSS and it can be mathematically written as in Equation (1) as seen in [15][9].

$$G_i(S) = \frac{V_{PSS_I}(s)}{d\omega_i(s)} = KG_i \frac{sT_w}{1+sT_w} \frac{(1+sT_{1i})}{(1+sT_{2i})} \frac{(1+sT_{3i})}{(1+sT_{4i})} \tag{1}$$

The structure consists of a control gain $Kpssi$, a washout filter constant TW, two lead-lag blocks for phase compensation with parameters $T1i$, $T2i$, $T3i$ and $T4i$ and a limiter. $VPSSi$ is the PSS output signal that goes into the generator exciter input. $\Delta\omega i$ is the generator speed deviation used as the PSS input signal[16].

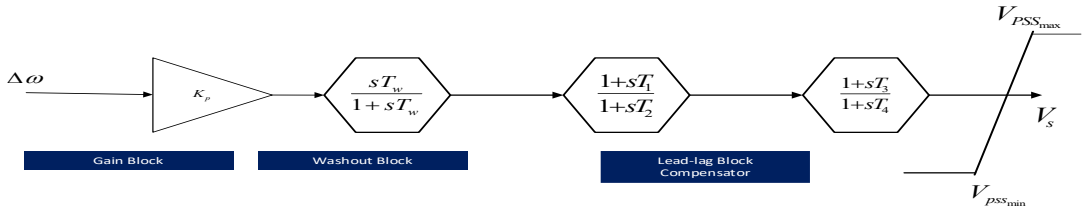

Figure 2.6 *Block diagram of a conventional lead-lag PSS[16]*

2.4.1 Damping controller design and performance

The damping of a power system can be improved by introducing a PSS loop into the excitation control system of a synchronous generator. PSS in the synchronous generator is considered as a supplementary block of the automatic voltage regulator (AVR) to produce component of damping torque in phase with the rotor angle deviation. The PSS always produces positive damping while AVR provides negative damping and synchronizing torque to the system. To improve the dynamic performance of the system. Its objective is to control oscillatory modes in the system[5]. The inclusion of PSS controller operation results in a higher damping ratio, which in turn results in faster stabilization of oscillations. Figure 2.7 shows the PSS controller coupled to the excitation system of the synchronous generator**.**

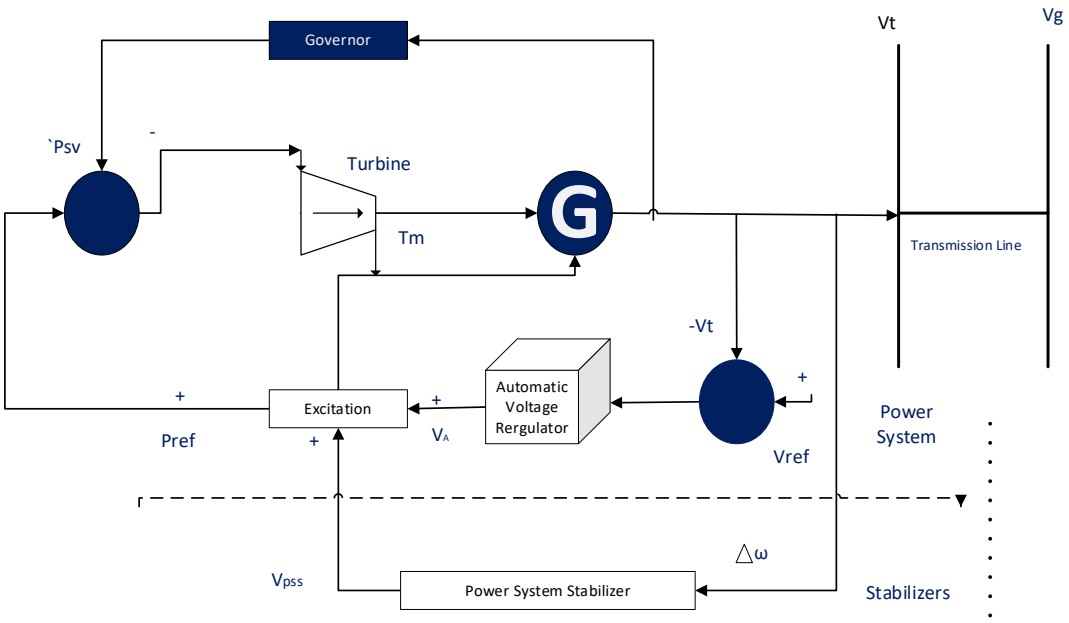

Figure 2.7 *PSS & AVR with Excitation System in the synchronous generator*

Presently, conventional PSS design for a specific operating condition may not cope with the dynamic nature of modern integrated power systems where operating conditions vary under wide operating ranges. Therefore, the parameters of the PSS are optimized to improve its efficiency in electromechanical oscillation damping. Due to its fast computational nature and ability to explore the optimal or near-optimal solution to the optimization problem, meta-heuristic techniques are deployed in PSS design.[5][17], [18].

2.5 Review of metaheuristics optimisation techniques

The term "metaheuristics" refers to a "higher level of heuristics" and is a combination of the words "meta" and "heuristic," where "meta" means beyond or higher level and "heuristic" refers to finding or discovering a goal by trial and error. Metaheuristic algorithms are optimization algorithms that are used to find the optimal solution for complex problems that cannot be solved using traditional methods. These algorithms are inspired by natural phenomena such as genetics, swarm behaviour, and evolution, and they are used to find the global optimum of a problem by exploring a large search space. Some popular metaheuristic algorithms include genetic algorithms, particle swarm optimization, ant colony optimization, simulated annealing, and tabu search etc. These algorithms have been widely used in various fields such as engineering, finance, and computer science to solve complex problems. One of the advantages of metaheuristic algorithms is that they do not require an initial starting point for the optimization problem. This makes them particularly useful for solving complex problems where the initial conditions are known. Additionally, metaheuristic algorithms can handle large and complex search spaces, which traditional optimization methods cannot. However, one of the main drawbacks of metaheuristic algorithms is that they may not always find the global optimum due to the random nature of the algorithm, there is no guarantee that the algorithm will find the best solution. Additionally, the algorithms can be computationally expensive, especially when dealing with large search spaces[19]. Figure 2.8 is a chart showing the classification of metaheuristic algorithms

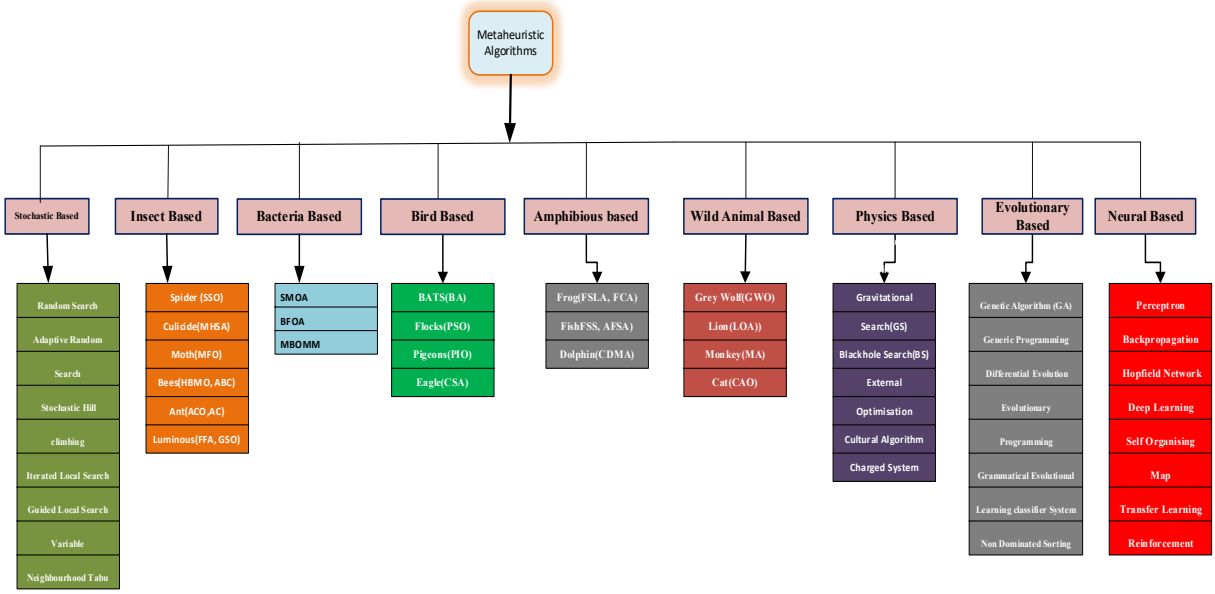

Figure 2.8 Chart of classification of Meta heuristics algorithms.

2.5.1 Review of Transit Search Algorithm

Transit search Optimisation Algorithm is novel astrophysics inspired metaheuristic algorithm based on exploration of exoplanets methods. There are five techniques or methods often used in exoplanet exploration. These are, Radial velocity method. Transit method, Direct imaging, Gravitational microlensing and Astrometry. As at March 2022, 915,384,558,129 and 1 planets have been discovered respectively. Therefore, the transit method has shown more potential so far than the second placed Radial Velocity Method.

Due to the high efficiency in astrophysics and the capabilities of this technique has led to the development of an optimisation technique for use in computational optimisation.

A galaxy is a collection of dust, gas, and billions of stars that are all held by gravity and revolves around its centre of mass. It also includes planets orbiting a host star as can be seen in the solar system. It is not expected that all of the regions of a galaxy be habitable. It is clear that the solar system as the place where we live is located in the life belt of the Milky Way galaxy. Exoplanets are planets that are outside the solar system and orbit a star other than the sun. One of the challenges for physicists is identifying exoplanets. The transit method as discussed above us the most successful technique in discovering exoplanets.

In this technique, starlight has observed by a space telescope is examined. By receiving the recorded information, changes in the brightness of the star over time are evaluated. If a planet passes between the observer (telescope) and the host star, the star's brightness decreases by a very small amount. Using this approach, scientists identify planets with different properties. The transit method is illustrated in Figure 2.9 based on the brightness received from the star during the time. The period of the planet can also be determined based on the number of passes. Many planets have been discovered so far. However, identifying planets alone is not important. The most important challenge is to find planets that can host life.

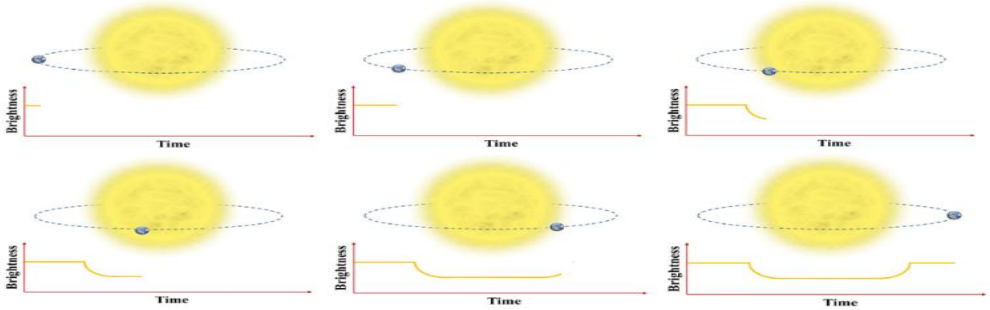

Figure 2.9 *Transit of planet around its star[19]*

2.5.2 Structure of the TS algorithm

There are five phases for implementing the TS algorithm, which include the phases of galaxy, star, transit, planet, neighbour, and exploitation. Further details of the structure of the algorithm can be found in[20]. Figure 2.10 shows the process flowchart of the Transit search algorithm.

Figure 2.10 Flowchart of the Transit Search Algorithm[19]

2.6 Objection Formulation

The primary goal of the objective function is to minimise Low Frequency Oscillations (LFOs) and improve power system stability during various disturbance conditions. The formulation of the objective function is therefore very critical in damping controller design, hence evaluating comparative performance under a common base is significant. The two common objective functions are eigenvalue and time-based error functions. In eigenvalues, the purpose of the objective function formulation is to shift eigenvalues efficiently to the deeper left-hand side of the complex s-plane. Two main players in the Eigenvalue objective functions are expressed in terms of the damping ratios and the real part of the eigenvalues. The eigenvalue objective function was employed to enhance the damping characteristics of electromechanical modes (EMs) in the system and shift the eigenvalues of the power system to the left region of the complex s-plane. The gain and parameters of the PSS are determined through the defined eigenvalue objective function as follows in Equation 2 from the study[20].

$$J = max\{real(\lambda_i)|\lambda_i \epsilon EMs\} + P_c \sum \{real(\lambda_i)|\lambda_i > 0\}$$

$$EMs = \left\{\lambda_i|0 < \frac{im(\lambda_k)}{2\pi} < 5\right\} \qquad (2)$$

Subject to $0.001 \leq K_{pssi} \leq 50$ and $0.001 \leq T_{1i} \leq 1$, $0.02 \leq T_{2i} \leq 1$, $0.001 \leq T_{3i} \leq 1$ and $0.02 \leq T_{4i} \leq 1$. The eigenvalue of the system state matrix is denoted by λ_i, PC is a penalty constant that penalizes the modes with an unstable eigenvalue [20]. In this study, PC is considered to be 50.

2.7 Review of Related works

The author of [21] developed a multistage optimisation technique by using the particle swarm optimization algorithm to improve the energy penetration and small signal stability in a power system. The work aims to improve the penetration levels of both wind and solar integrated power system. The work is in two stages, the first stage involves the use of the particle swarm algorithm to maximise the penetration levels of the renewable energies into the test system. The second stage involves improving the small signal stability of the test system with the improved penetration of renewable energy. The best location for citing the wind farm was also determined by the calculating the wind farm placement index and solar generation is fixed by considering voltage and load bus absorption capability.

The author of [22] used the Artificial Ecosystem Optimization(AEO) algorithm to tune an optimal power system stabiliser in a Single Machine Infinite Bus (SMIB) and Western Electricity Coordinating Council (WSCC) test system. The PSS design was considered as an optimisation problem and the eigenvalue-based objective function was employed. The aim was to improve the dynamic performance by improving the damping of electromechanical nodes. The performance of the AEO was validated by comparing the results with Generic Algorithm based power system stabilizer and Particle Swarm Optimisation based power system stabilizer. The simulations were done in the MATLAB/Simulink environment.

The author of [17] considered a power oscillation damper (POD) within the solar PV station for the effective damping of low frequency oscillations. The parameters of this controller is coordinated with the power system stabiliser of the single machine infinite bus system (PSS). In this paper, the PSS and the POD parameters were designed optimally with the PO(Political) heuristic algorithm. The PO method has been applied effectively here to design a supplementary damping controller via the active power control loop of a bulk PV station.

The author of [5] designed an optimal power system stabiliser with the Farm Fertility Algorithm (FFA) in an interconnected multimachine power system. The proposed FFA optimisation method was used to find the optimal control parameters of the PSS that are connected to the well-known IEEE 10-machine, 39-bus New England power system as the test system.

The author of [16] applied the FFA optimisation on the Western System Coordinated Council (WSCC) three machine nine bus power system. MATPOWER software was utilized to execute the system power flow which computes the system's initial condition states while the DAEs are solved via an ODE solver in MATLAB/SIMULINK.

The author of [2] on the impact of integrating very large-scale photovoltaic power plants on rotor angle and frequency stability affirmed that the increased penetration of large-scale renewable generation significantly affects the power system dynamic characteristics. The paper studied the effect of integrating very large-scale photovoltaic power plants on the power system rotor angle and frequency stability. An aggregate and detailed model including all dynamics and control loops, and effective components are proposed for VLS-PV generation systems. By using this model and other dynamic constituent of power systems, small signal and transient rotor angle stability, and frequency stability studies are performed on IEEE 39-bus and 118-bus test systems. The small signal stability is investigated through linearizing differential-algebraic system equations around the system operating point and then analysing eigenvalues of the state matrix of the system and the right and left eigenvectors associated with each eigenvalue. The modal analysis has been carried out using DIgSILENT Power Factory, a power system analysis software, for the default operating point of the 39-bus system. The paper concludes that the prediction of impacts of replacing/adding VLS-PV systems on the dynamic characteristic of the power systems is not possible as it requires extended studies by designing a complete set of scenarios of operation, disturbance, PV replacing/adding, control modes, and PV penetration. The author of [13] applied the Collective Decision Algorithm(CDO), Grasshopper Optimisation Algorithm (GOA) and Salp Swarm Algorithm (SSA) for the optimal tuning of PSS parameters for the small signal stability of a renewable integrated power network. The parameters were tuned with the metaheuristics algorithms with the aim of minimising the real part of the eigenvalues associated with the electromechanical nodes towards the deeper left hand of the complex S-plane and enhancing the damping ratios. Comparison of the result shows the superiority of the SSA over the CDO and GOA to boost the overall system stability over a wide range of operating conditions. The WSCC 3-Machine 9-Bus test system was used to carry out eigenvalue analysis when subjected to different operating/loading conditions and were coded in MATLAB platform. Case 1 was in respect of the PSS parameter tuning in which the results obtained were the eigenvalues and the damping ratio for different loading conditions. Case 2 in this paper involved the System's Time Domain Response for Case 1. To do this, a 3-phase fault was applied on one of the buses. A study of the change in speed deviation was used to reach a conclusion regarding the system stability. Case 3 involved the integration of renewable (PV) and case 4 involved the integration of PSS with PV.

The author of [23] tested on the New England 10-machine, 39-bus power system and considered severe operating conditions (line outages, load increases), compared single-objective vs. multi objective GA-based designs and evaluated performance using eigenvalue analysis and nonlinear time-domain simulations. The key results showed that the multiobjective GA-based PSSs achieved better damping of both local and inter-area oscillations and outperformed the single-objective designs by meeting stability and time-domain performance requirements simultaneously. Nonlinear simulations confirmed faster settling and superior damping under disturbances.

The author of [24] investigates five meta-heuristic optimization algorithms for designing Power System Stabilizers (PSSs) in multi-machine smart power systems. The goal is to improve damping of low-frequency electromechanical oscillations to enhance system stability and reliability. The paper shows that mathematical optimization algorithms provide superior performance in stabilizing smart power systems compared to nature-inspired methods.

The author of [25] proposed a new Collective Decision Optimization (CDO) algorithm for optimal PSS design. The CDO is compared with other metaheuristic algorithms such as Grey Wolf Optimizer (GWO), Differential Evolution (DE), Whale Optimization Algorithm (WOA), and Crow Search Algorithm (CSA). The eigenvalue analysis is then used to evaluate system stability and damping ratios. The test systems for this study is the WSCC 3-machine 9-bus and IEEE 14-bus systems.

The author of [26], as part of advanced approaches identified Wide-area damping controllers, FACTS devices, artificial intelligence & Fuzzy Logic. The paper emphasizes that while conventional PSSs have been effective in the past, modern interconnected grids with renewables and complex dynamics require adaptive, AI-driven, and wide-area coordinated stabilizers to ensure reliability and prevent large-scale blackouts.

The author of [27] proposed a PID-based Power System Stabilizer (PIDPSS) for damping low-frequency oscillations (LFOs) and improving angular stability in a Single Machine Infinite Bus (SMIB) power system. A novel Farmland Fertility Algorithm (FFA), a nature-inspired metaheuristic algorithm is introduced to optimally tune PIDPSS parameters with the results compared against conventional PIDPSS (CPIDPSS) tuned by trial-and-error and the Differential Evolution (DE) algorithm tuned PIDPSS.

FFA PIDPSS outperformed DE and CPIDPSS in terms of Faster convergence (69 iterations vs. 77 for DE), improved transient response metrics; rise time improved by 37.37%, settling time improved by 33.73%, peak time improved by 7.36%, ISTSE reduced by 6.26% compared to DE.

The author of [28] proposed a POD controller for Converter Interface Generators (CIGs, solar wind, etc) that uses both active and reactive power injection. The controller adapts automatically when network topology changes (e.g., faults, line disconnections) while adaptation is based on monitoring oscillation frequency and adjusting controller parameters in real time. The test system was both tested in a laboratory setup with four 15 kVA converters and a 75 kVA grid emulator and also applied to the IEEE 39-bus system in simulations. The results revealed that combined active + reactive power control gave best damping performance, especially under reconfiguration.

The author of [29] used PSCAD/EMTDC simulations and confirmed that theoretical predictions for improper parameter settings lead to instability. The paper highlights that two-stage PV systems have unique LFO behaviours strongly influenced by DC–DC converter, inverter voltage control, and PLL dynamics, and careful tuning of control parameters plus consideration of grid impedance is essential for stability.

The author of [30] reviewed wide-area damping control (WADC) for restraining inter-area low-frequency oscillations (LFEO) in large-scale power systems. The study affirms that Low Frequency Oscillations (LFOs) are a major barrier to dynamic stability and power transfer, especially with the rising penetration of wind and photovoltaic (PV) generation. The paper concludes LFOs are increasingly critical with renewable integration highlighting that WADC, supported by WAMS, offers a robust solution to enhance stability and increase renewable penetration.

The author of [31] proposed an AI-enhanced Power Oscillation Damper (MiPOD) that uses Random Forests to predict oscillation frequencies and enable grid-connected converters to damp multiple electromechanical oscillations, improving smart grid stability with minimal resources. Tested on the two-area Kundur system under various disturbances (short circuits, load changes, generator torque variations, topology changes), the results show that MiPOD significantly improves damping compared to conventional synchronous power controllers (SPC). Stability enhanced even when distributed power plants contribute only 6% of total generator capacity and the system settles faster after disturbances, with reduced oscillation amplitudes.

The author of [32] mentioned that the rapid growth of photovoltaic (PV) plants worldwide, especially in China, has raised concerns about power system stability due to the volatility and uncertainty of solar generation. High PV penetration can worsen interarea oscillations, making damping control essential. An Adaptive Wide Area Oscillation Damper (A-WPOD) was designed for PV plants using a Goal Representation Heuristic Dynamic Programming (GrHDP) which is a model-free, neural-network-based adaptive control method. This was tested on a 16-machine, 68-bus benchmark system with a 200 MW PV plant and the results show that A-WPOD adapts effectively to different operating conditions and contingencies with superior damping compared to conventional

lead–lag WPOD. The ADC successfully compensates constant, time-varying, and stochastic delays with online learning allowing A-WPOD to adjust weights dynamically during disturbances.

The author of [33] proposed that instead of designing two controllers separately, a coordinated design of multiple damping controllers DFIG POD and synchronous generator PSS was proposed. The hybrid optimization algorithm Grey Wolf Optimizer and Particle Swarm Optimizer was applied to tune the controller parameters while the multiobjective eigenvalue optimization ensures damping ratios meet stability thresholds. The test system was on a two-area four-generator benchmark system. The paper demonstrates that coordinated damping control using hybrid optimization is a superior strategy for stabilizing power systems with large-scale wind farms compared to traditional or uncoordinated methods.

The author of [34] concluded that PV systems, when equipped with proper active/reactive power control, can enhance transient stability and reduce losses. Local integration of PV at load centres improves reliability but requires careful management of voltage fluctuations. The methodology employed involves simulations conducted on a four-generator, 11-bus test system using DIgSILENT PowerFactory. Critical Clearing Time (CCT) is used as the stability indicator. Bisection technique was applied to evaluate minimum CCT under different scenarios.

Parvathy G. Manju Sreekumar in [35] compared the LQR (Linear Quadratic Regulator) with the LQG (Linear Quadratic Gaussian) controllers. Using the MATLAB environment, he modelled the PV arrays, multi-machine systems, and their integration into the grid. The paper concluded that LQG controller outperforms LQR in terms of rise time (faster response), settling time (quicker stabilization), overshoot (reduced oscillations) and steady-state error (maintained accuracy).

The author of [36] proposed a minimax linear quadratic Gaussian (LQG)-based power oscillation damper (POD) designed for PV plants. This controller aims to provide robust damping of interarea oscillations under varying operating conditions and uncertainties. The method includes system linearization, modal analysis, signal selection, incorporation of time delays and Riccati equation solution. The paper demonstrates that a minimax LQG-based POD integrated into large-scale PV plants can robustly stabilize interarea oscillations, even under uncertainties and delays, offering a better solution than conventional controllers.

2.7.1 Summary of Review

The literature reviewed implies that:

i. the integration of renewables into the conventional grid is imminent and the need for continuous analysis and research in terms of stability of the grid would need to continue.
ii. The use of damping controllers in the power grid system to damp out and control low-frequency oscillations can no longer be overemphasised. The PSS damping controller is coupled to the generator excitation systems to control these oscillations. However, the PSS needs to be optimally designed.
iii. The use of metaheuristics algorithm to optmise the power system stabiliser which is used to damp out low frequency oscillations.

2.8 Focus of the work

This chapter has provided a good theoretical review and literature review of related works, which supports this research work. The theoretical background presented takes into account the analytical evaluations undertaken in the succeeding chapters. This research fills the gap by studying a power system with a Solar (PV) renewable system integrated using the WECC model and to analyse the impact on stability with respect to the rotor angle. The thesis will also introduce the Transit Search (TS) optimization algorithm to optimally design the PSS damping controller.

3.1 MATERIALS AND METHODS

This chapter discusses the method process and the mathematical formulations used in this research. The various mathematical formulations for the power system modelling were adopted from studies [21], [37],[38],[20]. Figure 3.1 shows the flowchart of the step-by-step procedure for the research. Detailed modelling of the power test systems for rotor angle stability study in the MATLAB/SIMULINK environment is presented. The various power system models including the WECC validated Distributed Station Solar PV model and data are adopted from [20], [37], [14]. A single- machine infinite bus system (SMIB) is adopted as the test system to depict the conventional power system model while a Solar PV energy conversion system is used to relate the renewable power system model. All the system model are adopted from (K.Muhammad 2020)

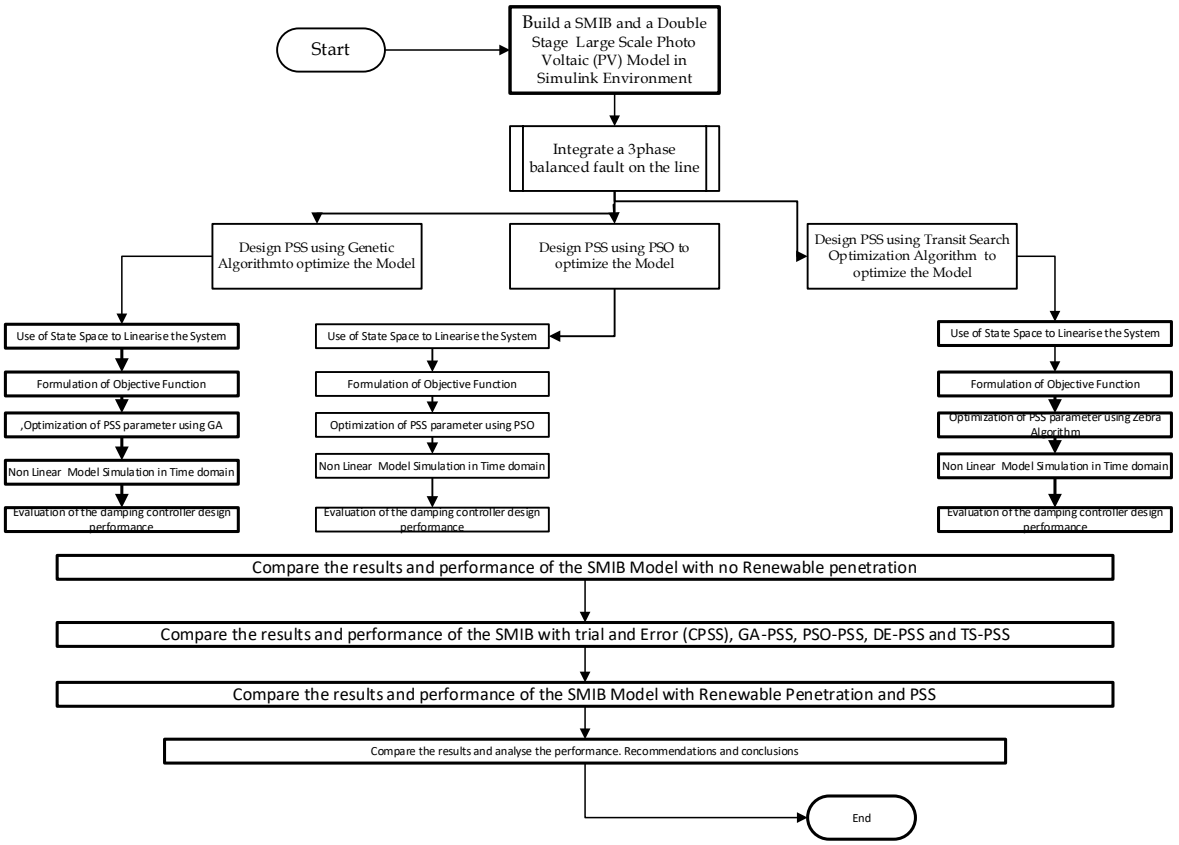

Figure 3.1 *Flow Chart of the Design Process for this Research*

3.2 EQUIPMENT

The simulations of this research work were conducted using MATLAB/SIMULINK software R2020a on a HP 240 G8 Notebook PC, Intel(R) Core (TM) i3-1005G1 @ 1.2GHz, 64bit Operating System on Windows 10 Home.

3.3 Design Building Blocks Process

3.3.1 Single Machine Infinite Bus Test System (SMIB)

An infinite bus is a bus which has a fixed voltage (both magnitude and phase angle) and frequency; therefore, the infinite bus can be used to represent a connection to a strong grid which will absorb the injected power at the infinite connection point without a noticeable change in the voltage or frequency. A typical three phase synchronous machine consist of the stator with armature windings and rotor, either cylindrical or salient pole, with field windings with the stator and rotor separated by a small air gap enough to have a clearance. In respect to the rotor shape and airgap, there exist two axes of symmetry. These two axes are named the d-axis and q-axis and the rotor rotates relative to the stator, self and mutual inductances are induced by time-varying fluxes between the armature and rotor circuits. In synchronous machine modelling, the time-varying inductances complicate the model but dq transformations are used to simplify the model. The synchronous machine is modeled using Differential Algebraic Equations (DAEs). The solution loop of the SMIB generator system is shown in Figure 3.2.

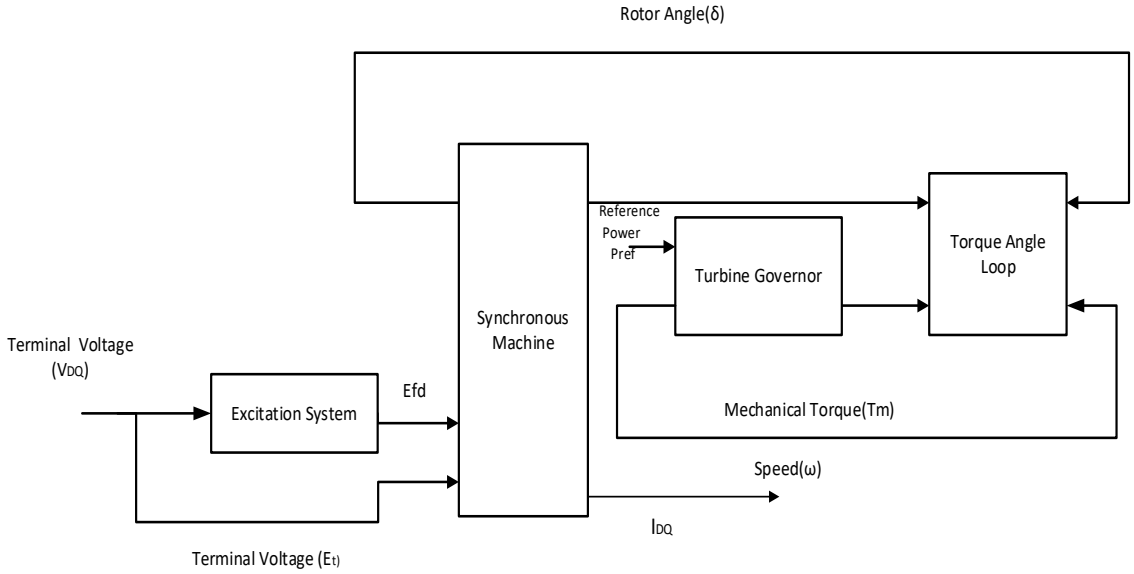

Figure 3.2 *Single Machine Infinite Bus Solution Loop*

The terminal Voltage (V_{DQ}) is the input voltage to the generator through the excitation system obtained from the network block while the output of the generator is the current I_{DQ} which is fed to the network block. The generator block consists of the mechanical and electrical side. The mechanical side is represented by the Torque Angle Loop while the electrical side is represented by the Synchronous machine block.
From the flowchart in figure 3.1, it is pertinent to note that to run time domain simulations for the SMIB system, there is need to create Simulink model that represents the infinite bus, the line and the synchronous machine. In the following sections, the various Simulink blocks that make up the SMIB solution is further explained.

3.3.1.1 Excitation System

The excitation systems involve the regulation of the generator bus voltage by adjusting the generator field. The Simulink representation of the excitation block is shown is Figure 3.3 and a simple static excitation system equation is placed as equation 3.

$$\frac{dE_{fd}}{dt} = \frac{1}{T_a}\left(K_a V_{ref} - K_a E_t - E_{fd}\right) \quad (3)$$

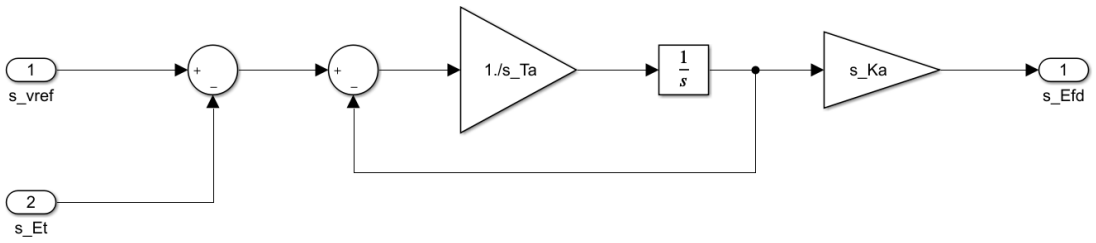

Figure 3.3 *Simulink representation of Excitation Block as in Equation 3*

3.3.1.2 Torque Angle Loop: The Torque Angle loop is presented as Figure 3.4 and represents the generator mechanical dynamics as expressed in equation 4. This describes the rotor angular speed due to a mismatch of torques in the mechanical system.

$$\frac{d\delta}{dt} = \omega_b(\omega_r - \omega_s)$$
$$\frac{d\omega_r}{dt} = \frac{1}{2H}\left(T_m - T_e - D(\omega_r - \omega_s)\right) \quad \text{.....4}$$

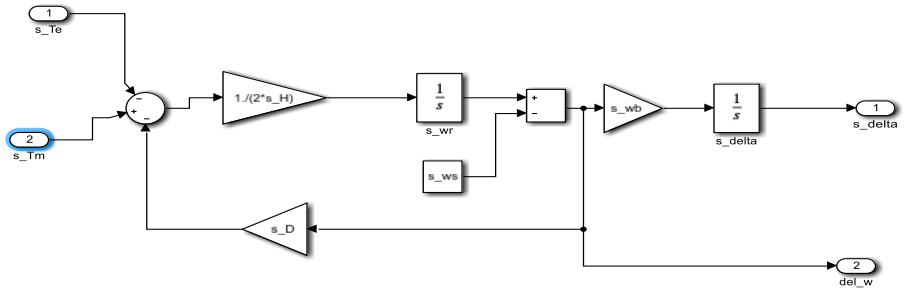

Figure 3.4 *Simulink representation of the Torque Angle Loop*

3.3.1.3 Turbine Governor: The function of the turbine governor is to regulate the system frequency during changes such as change in generator load by adjusting the input torque to the generator. Equation 5 shows the equation for the turbine governor while Figure 3.5 shows the Simulink representation.

$$\frac{dT_m}{dt} = \frac{1}{T_g}\left(T_{m2} - T_m - \frac{\omega_r - \omega_s}{R_{gov}}\right) \text{.....5}$$

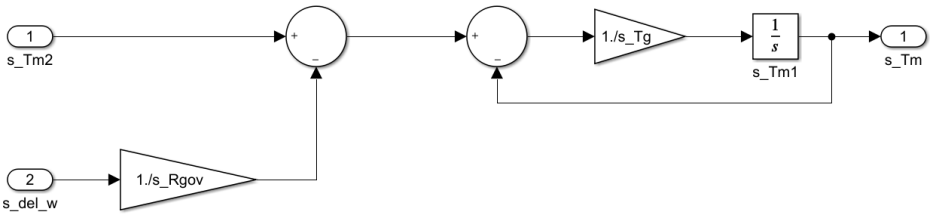

Figure 3.5 *Simulink representation of Turbine Governor Block*

3.3.1.4 Synchronous Machine: This is the electrical side of the SMIB generator system. The machine equations are divided into (a), electrical torque (Te), (b), the q and d-axis stator current components, (c), Transient EMF due to field in d and q-axis damper coil flux linkage, (d), sub-transient EMF due to flux linkage in d and q axis.

a) Electrical torque: The electrical torque can be obtained from the electrical equations of the machine as shown in Equation 6 and the Simulink representation in Figure 3.6

$$T_e = \frac{x''_d - x_{ls}}{x'_d - x_{ls}} E'_q I_q + \frac{x'_d - x''_d}{x'_d - x_{ls}} \psi_{1d} I_d + \frac{x''_q - x_{ls}}{x'_q - x_{ls}} E'_d I_d - \frac{x'_q - x''_q}{x'_q - x_{ls}} \psi_{2q} I_d + \left(X''_q - X''_d\right) I_d I_q \qquad (6)$$

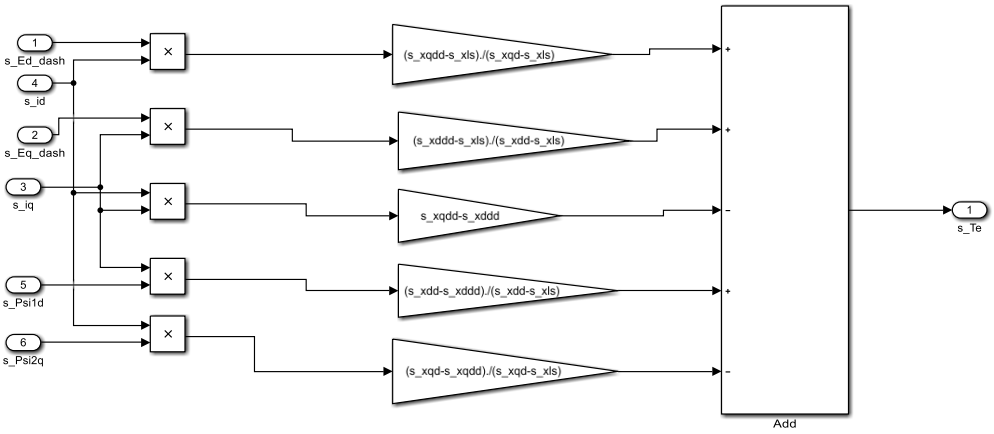

Figure 3.6 *Simulink representation of electrical Torque as in Equation 6*

b) The q and d-axis stator current components are represented by Equation 7 & 8 respectively:

$$I_q = \frac{R_s}{R^2{}_s + X''^2{}_d}\left(E'_q \frac{X''_d - X_{ls}}{X'_d - X_{ls}} + \psi_{1d}\frac{X'_d - X''_d}{X'_d - X_{ls}} - V_q\right) + \frac{X''_d}{R^2{}_s + X''^2{}_d}\left(E'_d \frac{X''_q - X_{ls}}{X'_q - X_{ls}} + \psi_{2q}\frac{X'_q - X''_q}{X'_q - X_{ls}} - V_d\right) \quad (7)$$

$$I_d = \frac{R_s}{R^2{}_s + X''^2{}_d}\left(E'_d \frac{X''_q - X_{ls}}{X'_q - X_{ls}} - \psi_{2q}\frac{X'_q - X''_q}{X'_q - X_{ls}} - V_d\right) - \frac{X''_d}{R^2{}_s + X''^2{}_d}\left(E'_q \frac{X''_d - X_{ls}}{X'_d - X_{ls}} + \psi_{1d}\frac{X'_d - X''_d}{X'_d - X_{ls}} - V_q\right) \quad (8)$$

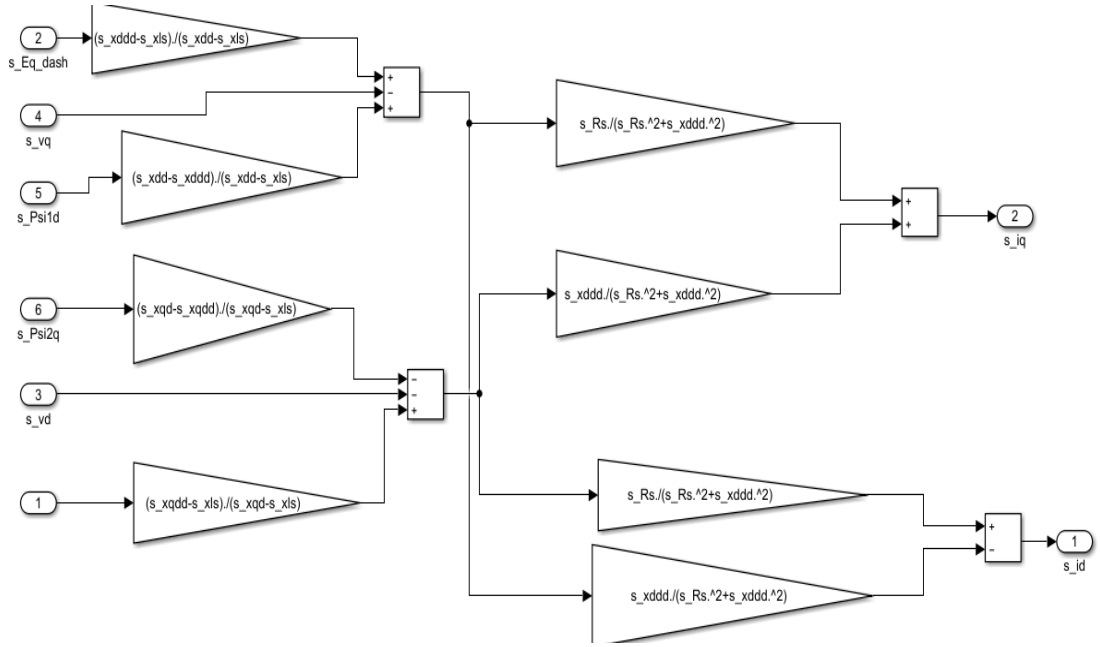

Figure 3.7 *Simulink representation of q and d axis stator components, Equation 7 and 8*

c) Transient EMF due to the field in d and q axis damper coil flux linkage, are represented in q axis by Equation 9 while the Simulink representation is shown in Figure 3.8.

$$\frac{dE'_q}{dt} = \frac{1}{T'_{d0}}\left[-E'_q + E_{fd} + (X_d - X'_d)\left(I_d + \frac{X'_d - X''_d}{(X'_d - X_{ls})2}\{\psi_{1d} - E'_q - I_d(X'_d - X_{ls})\}\right)\right] \quad (9)$$

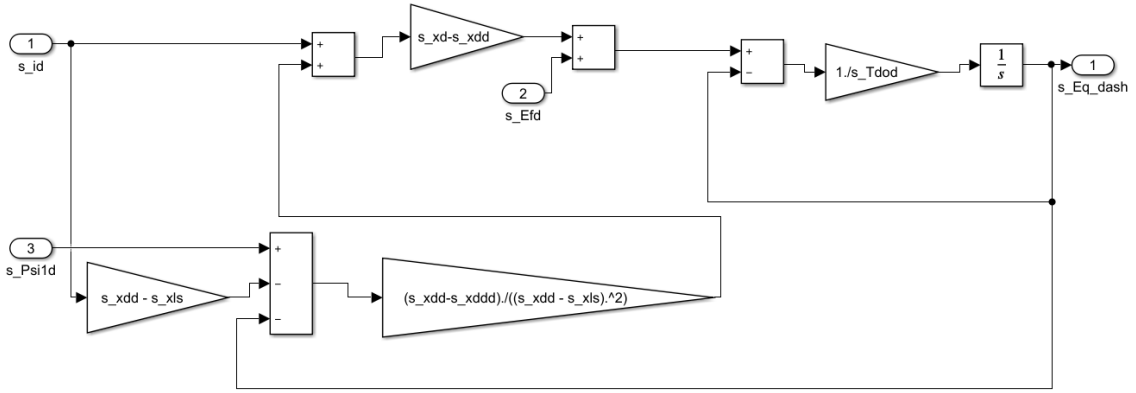

Figure 3.8 *Simulink representation of transient EMF due to flux-linkage in the q-axis as in Equation 9*

And in d axis by Equation 10 while the Simulink representation is shown in Figure 3.9

$$\frac{dE'_d}{dt} = \frac{1}{T'_{q0}}\left[-E'_d + E_{fq} + (X_q - X'_q)\left(-I_q + \frac{X'_q - X''_q}{(X'_q - X_{ls})2}\{-\psi_{2q} - E'_d - I_q(X'_q - X_{ls})\}\right)\right] \quad (10)$$

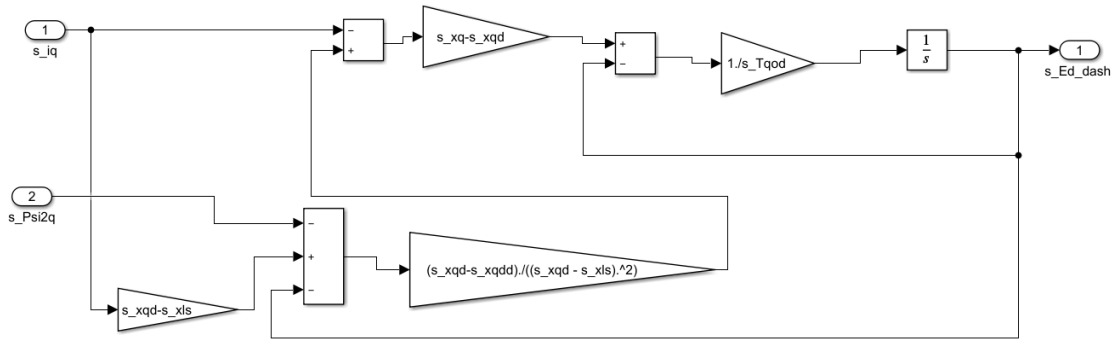

Figure 3.9 *Simulink representation of the transient EMF due to flux linkage in d-axis as in Equation10*

d) sub transient EMF due to flux linkage in the d and q axis is represented in the q axis by Equation 11 while the Simulink representation is shown in Figure 3.10.

$$\frac{d\psi_{2q}}{dt} = \frac{1}{T''_{q0}}\left(-\psi_{2q} - E'_d + I_q\left(\mathcal{X}'_q - \mathcal{X}_{ls}\right)\right) \quad (11)$$

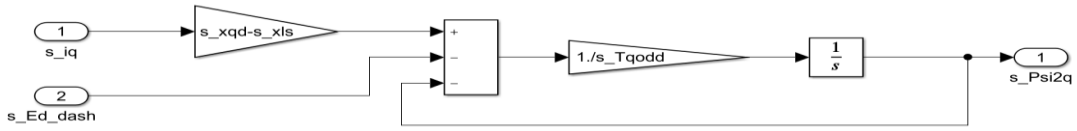

Figure 3.10 *Simulink representation of sub transient EMF due to flux linkage in q-axis*

And in the d-axis by Equation 12 while the Simulink representation is shown in Figure 3.11.

$$\frac{d\psi_{1d}}{dt} = \frac{1}{T''_{d0}}\left(-\psi_{1d} - E'_q + I_d(\mathcal{X}'_d - \mathcal{X}_{ls})\right) \quad (12)$$

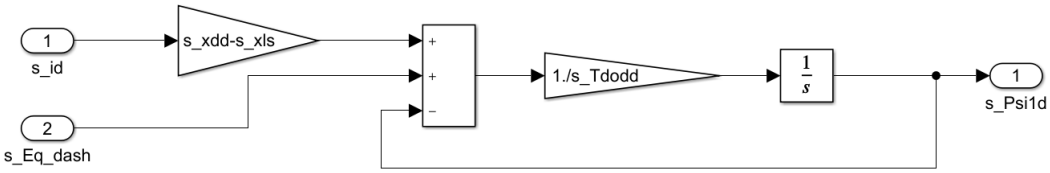

Figure 3.11 *Simulink representation of sub transient EMF due to flux linkage in d axis*

The subsystems developed so far from Figures 3.6 – 3.11 (Equations 6 – 12) can be described as the electrical side of the generator. The subsystems are then grouped as in Figure 3.12.

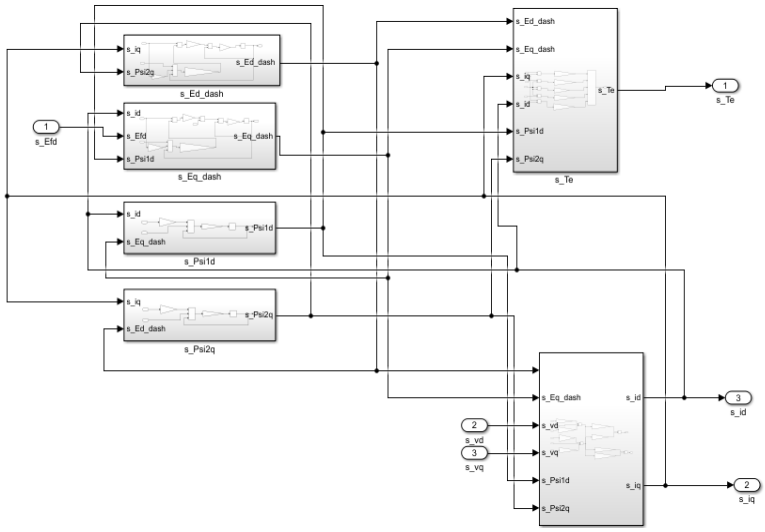

Figure 3.12 *Simulink representation of the Electrical Side of the generator*

The remaining part of the electrical side of the generator is the dq-frame of generators and the DQ-frame of the network from the network block. This conversion is necessary and has been derived and explained in the study [20] as reference frames. The generator receives voltage VDQ in DQ-frame, which is converted to dq-frame according to Equation 13. The current that comes from the generator is in dq-frame and needs to be converted back to DQ-frame for the network according to Equation 14.

DQ to dq block: Once the voltage is converted, it is split into its real (Vq) and imaginary (Vd) component as shown in the Simulink representation in Figure 13.

$$V_q + jV_d = \left(V_Q + jV_D\right)e^{-j\delta} \tag{13}$$

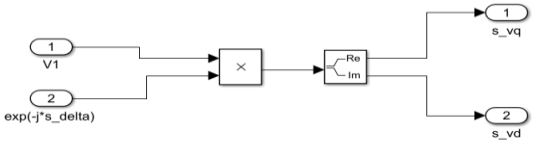

Figure 3.13 *Simulink representation for converting DQ to dq frame as shown in Equation 13*

dq to DQ block: The reverse process is used here to convert the current to a DQ-frame for the network as shown in the Simulink representation in Figure 14.

$$I_q + jI_d = \left(I_Q + jI_D\right)e^{-j\delta} \tag{14}$$

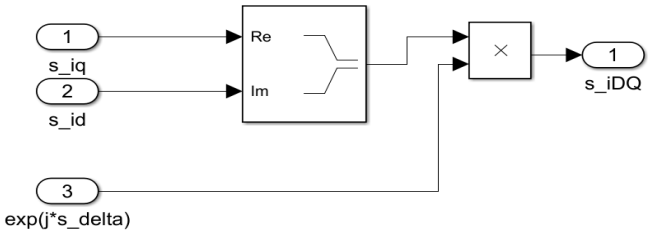

Figure 3.14 *Simulink representation for the dq to DQ conversion as shown in Equation 14*

Lastly, the Mathematical block for the DQ conversion creates the terms for the rotation of the phasors, here the angle (δ) is transformed $into\ e^{-j\delta}\ and\ e^{j\delta}$ as seen in Figure 15.

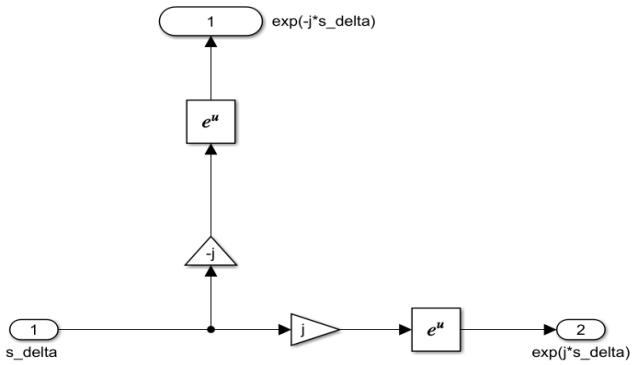

Figure 3.15 *Simulink representation of the mathematical block for exponentials*

The electrical side of the generator in Figure 3.12 and the reference blocks explained above are now grouped into a larger system that represents the electrical machine equations. The Simulink representation is shown in Figure 3.16.

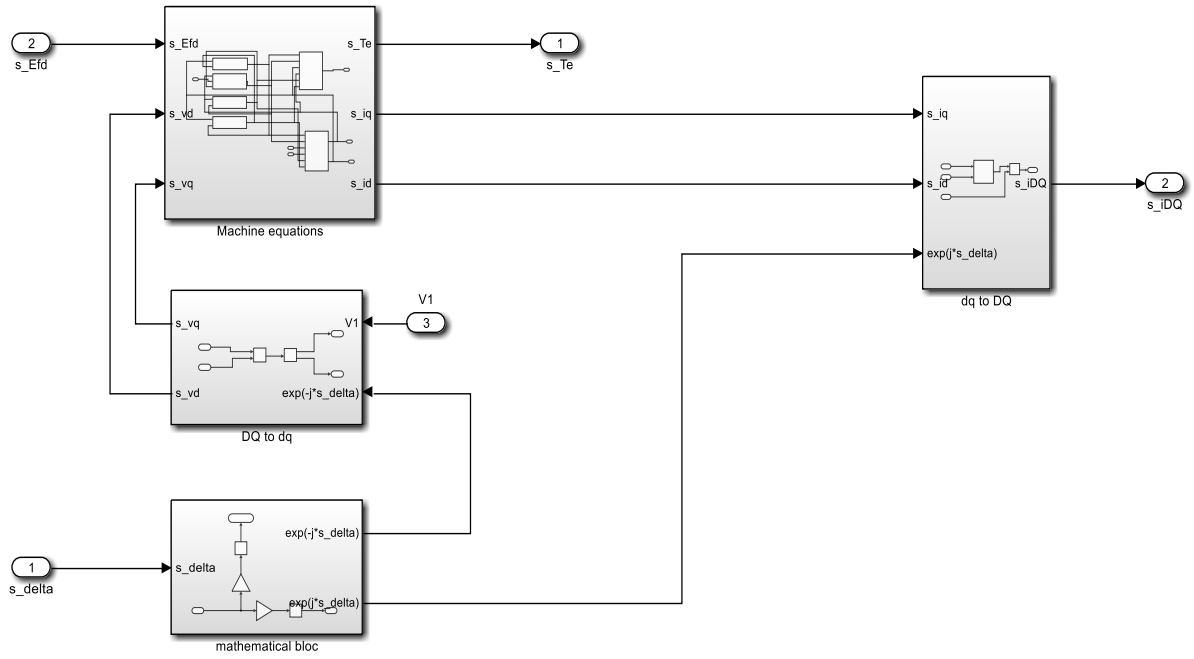

Figure 3.16 *Simulink representation of the Electrical Machine Block*

The mechanical and electrical sides, including the excitation, governor control system, torque angle loop complete the SMIB synchronous generator system. The inclusion of the Power System Stabiliser (PSS) which is connected to the excitation system is included to the solution loop of Figure 3.2. This is now represented in the Simulink model of Figure 3.17. Further elucidation on the PSS design is done in section 3.4.

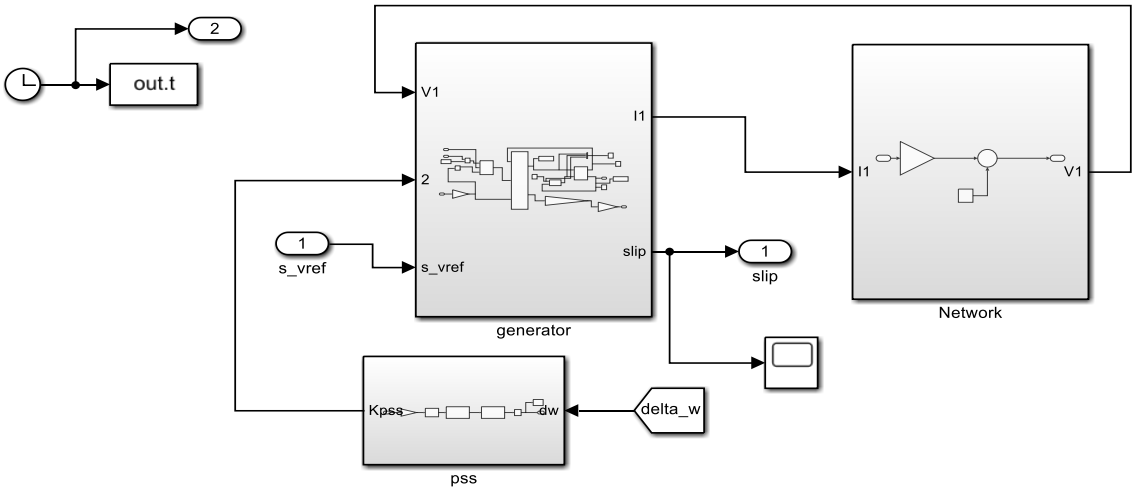

Figure 3.17 *Simulink representation of SMIB Generator with PSS Model*

3.3.2.1 Network for the SMIB

Equation 15 shows the SMIB Network equation. Where V_{inf} is the voltage at the infinite bus, there is a reciprocal relationship between the voltage and current as any changes in the current injection from the generator affects the network voltage, and also any changes in network voltage affect the generator. The Simulink representation is shown in Figure 18.

$$V_i = V_{inf} + I_1 * Z_{line} \text{.....} \quad (15)$$

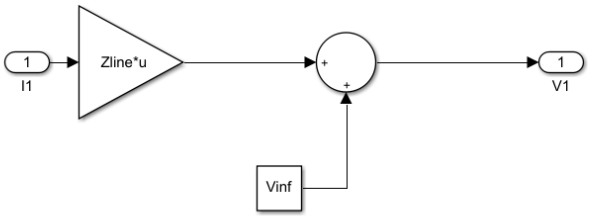

Figure 3.18 *Simulink representation of the Network*

The SMIB generator system in Figure 3.17 is attached to the network system in Figure 3.18 to complete the SMIB system in Figure 3.19.

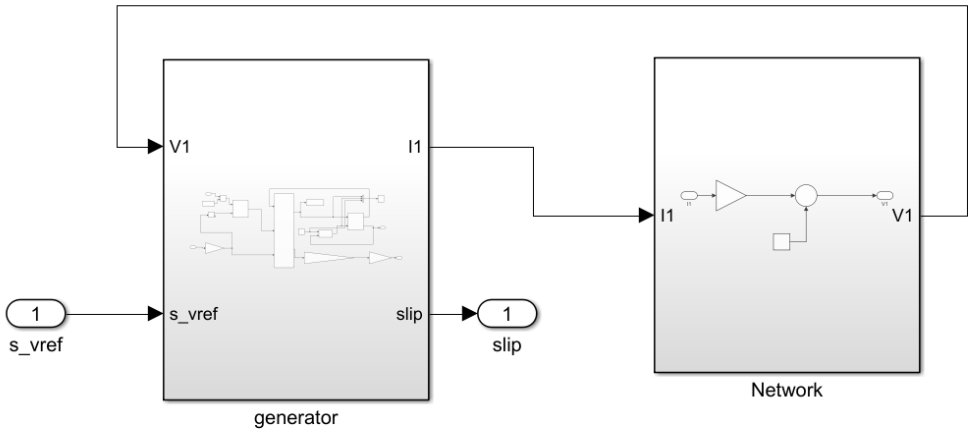

Figure 3.19 *Simulink representation of the complete SMIB Model without the PSS*

3.3.3.1 PHOTOVOLTAIC SOLAR MODEL

Wind generation and Photovoltaic (Solar) generation are the two most popular renewable energy generation technologies, still, PV generation is not yet developed as the Wind counterpart. The Western Electricity Coordinating Council (WECC) has therefore developed two generic PV generator models, one for very large PV plants connected at transmission level and a second model for distributed PV generation, connected at distribution level, suitable for transmission level studies. This thesis considers the distributed PV generation model which does not contain the plant controller module which is the major difference between it and the one for large PV plants. See Figure 2.4 in chapter two for the complete PV System model.

In general, the PV system can be separated into different components/subsystems for the ease of modelling. A simple diagrammatic view of the PV solar system is shown in Figure 3.20.

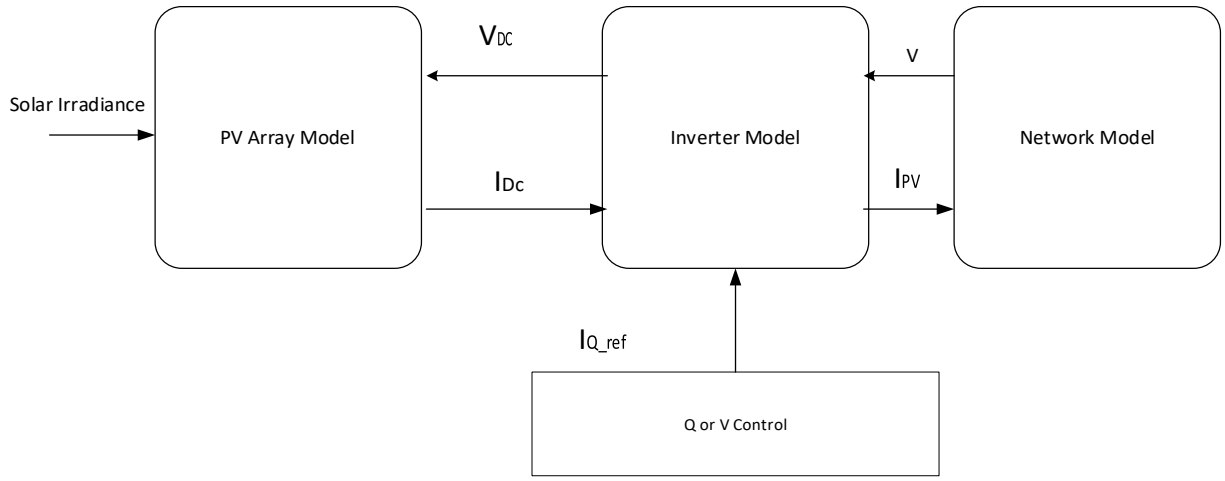

Figure 3.20 *Diagrammatic view of physical PV Model*

In this thesis, the model used does not include the PV array module which links relationship between solar irradiance with voltage and temperature change, instead available power is assumed to be a certain value and the focus of the model is on the electrical disturbances. According to the WECC document, the recommended integration time step is 1-10ms with a typical duration of simulation in the 30s range. Models are able to represent phenomena of up to 10Hz. The model should only be used down to 25% of rated power and an SCR of at least 2 at the point of interconnection[39]. The PV model is divided into seven subsystems which include delω to frequency, machine reference voltage, real power, reactive power, tripping, subsystem that converts the iq and ip commands to ip and iq and the system reference.

Delω to frequency: Figure 3.21 this block shows that we have selected the frequency of the nearby synchronous generator and converted it from the per unit difference to the nominal speed back to its synchronous speed in Hz. The delω is obtained in this case from the SMIB block.

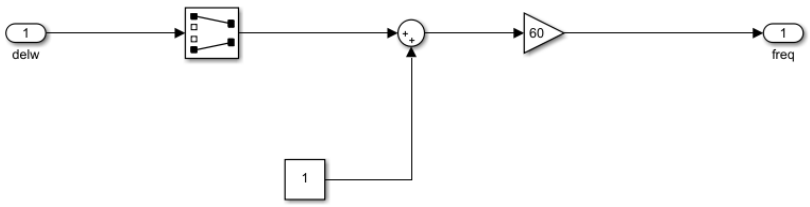

Figure 3.21 *Simulink representation of frequency of synchronous machine in Hz.*

Machine referenced voltage: Figure 3.22 shows the subsystem for the PV systems terminal voltage. While only the voltages at PV terminal buses are selected, the PV system model is aligned with its terminal voltage, such that only voltage magnitude is required inside the model. The voltage angle is now required for the back conversion to the network reference frame.

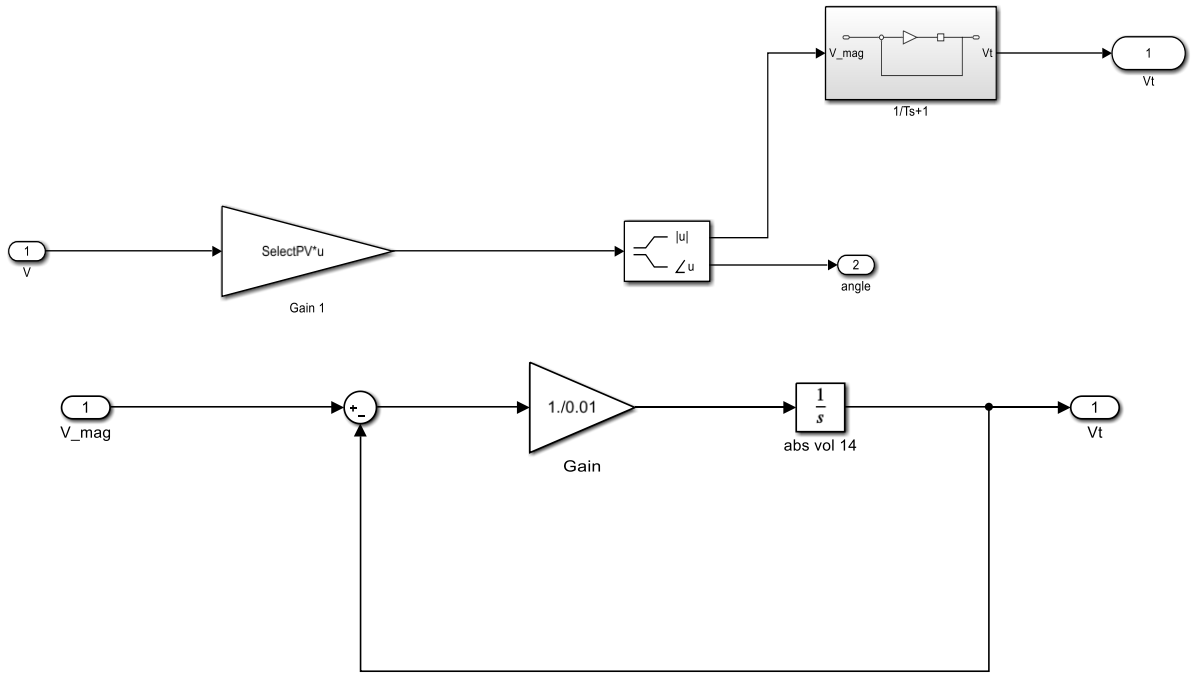

Figure 3.22 Simulink representation of the terminal voltage of the PV model

Real Power: Figure 3.23 is the real power block for the PV model. It shows that the total real power the PV system is generating is made up of the reference power, an additional droop setting in case of frequency control and the option for a supplemental active power signal Pext(zero by default). The droop setting includes a dead zone block, with the starting value set as f_{dbd} and the end value set to a very high value, here 10^20.

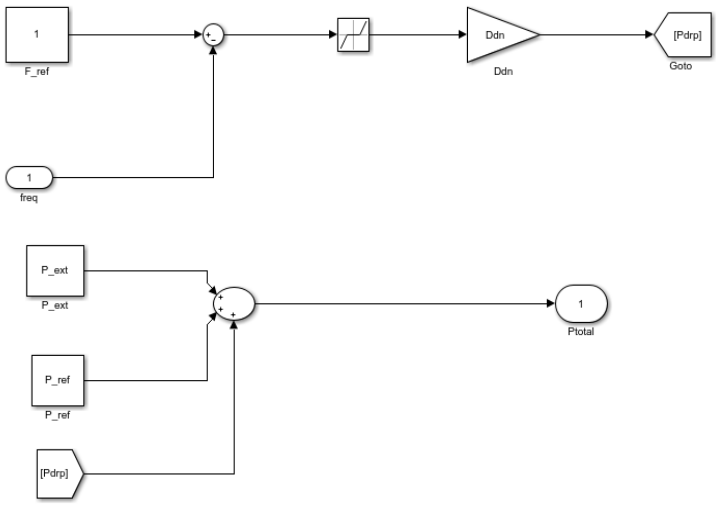

Figure 3.23 *Simulink representation of the real power instruction*

Reactive power: The reactive power is set to the reference value with the option to adjust the reference value to include a voltage droop or line drop compensation with the reactance value X_C. The dead zone block has a starting value of V_0*D_{qdv} and an end value of V_1*D_{qdv} while the saturation has an upper limit of Qmx-Qref and a lower limit of Qmn-Qref. This is shown in Figure 3.24

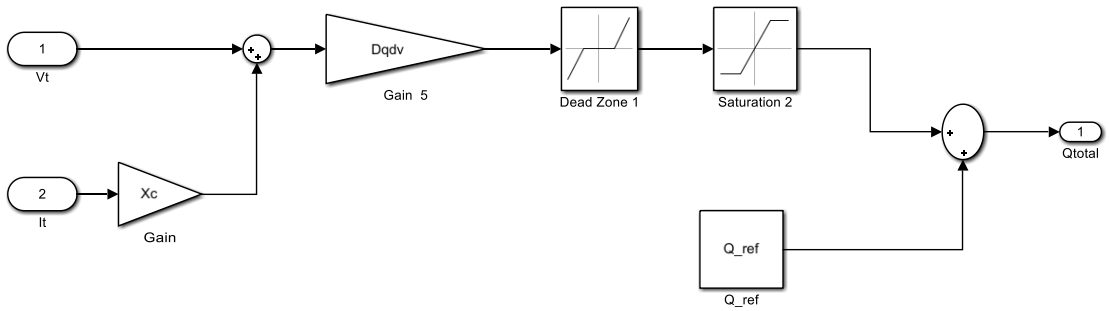

Figure 3.24 *Simulink representation of the reactive power instruction*

Flags for Tripping: The PV generation will trip during low voltage, high voltage and low or high frequency conditions. This tripping happens gradually, with a reduction of the connected PV output, as the situation worsens. Low voltage tripping is initiated from a voltage below Vt1 with total disconnection at a voltage level of Vt0, whereas high voltage tripping is initiated from a voltage level of Vt2 with total disconnection from a voltage level of Vt3, as shown in Figure 3.25

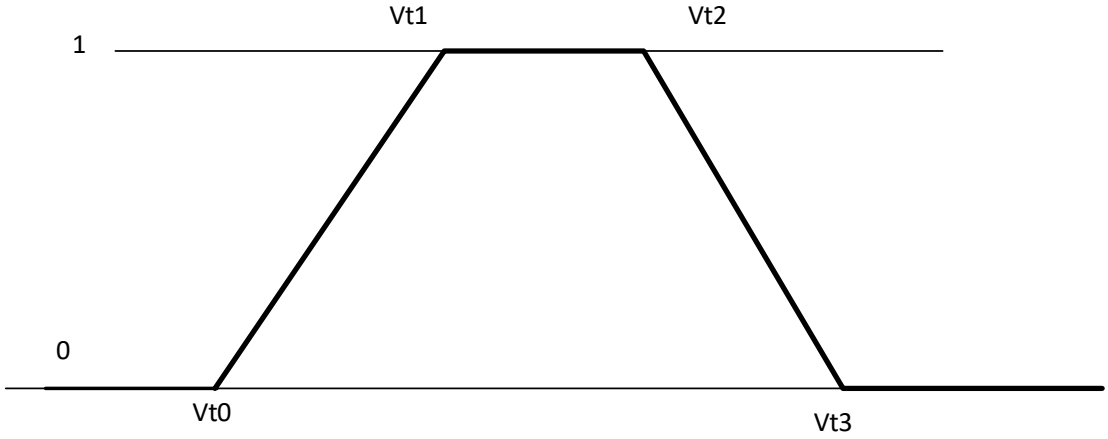

Figure 3.25 *Low and High Voltage tripping limits Vt0 to Vt3*

Low Voltage Tripping Flags:

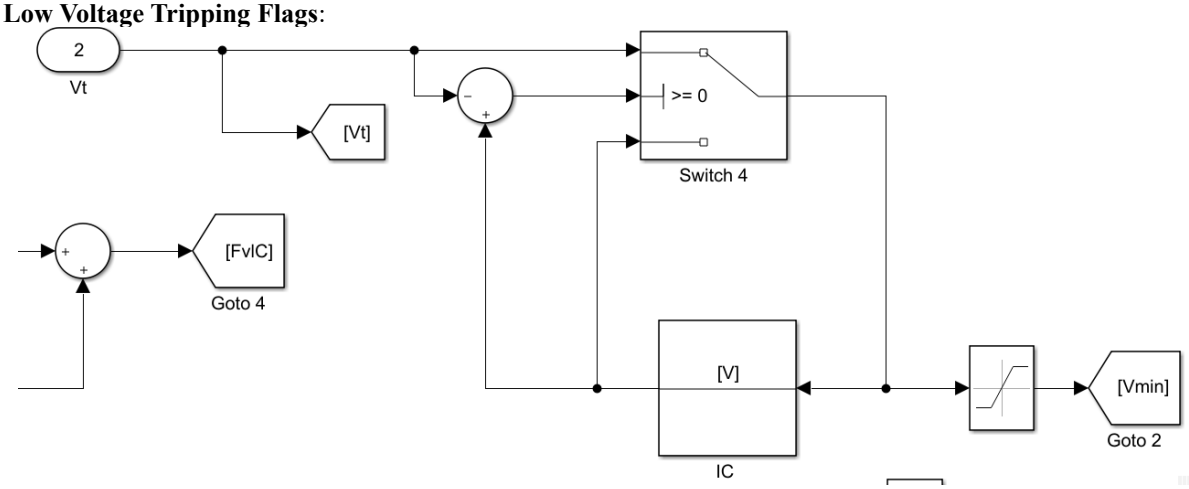

Figure 3.26 *Simulink representation of the Low voltage tripping, tracking lowest voltage* V_{min}

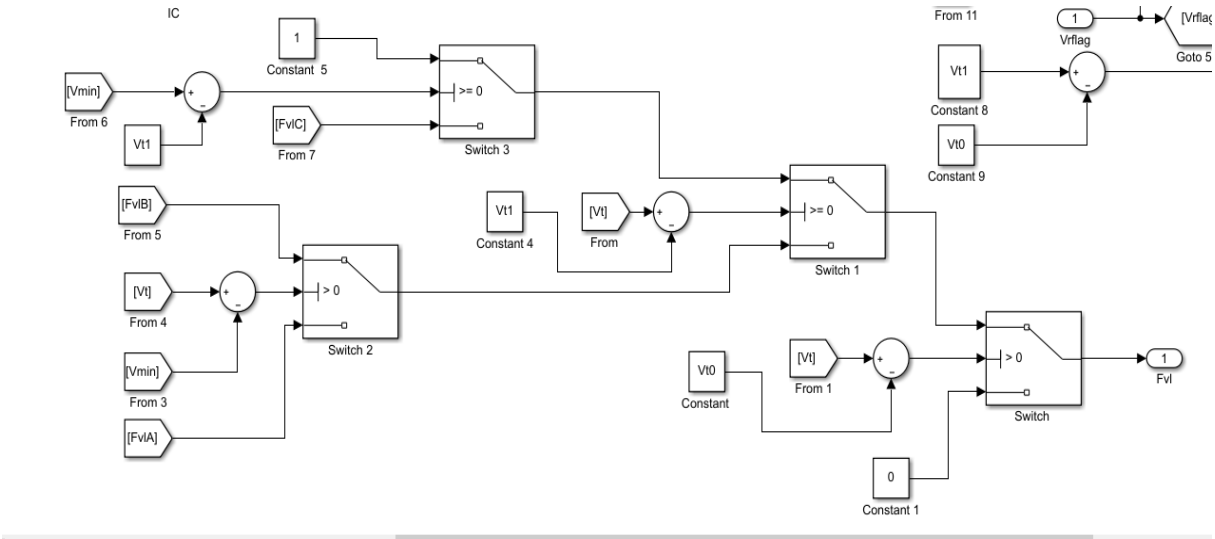

Figure 3.27 *Simulink representation of the Low voltage tripping logic*

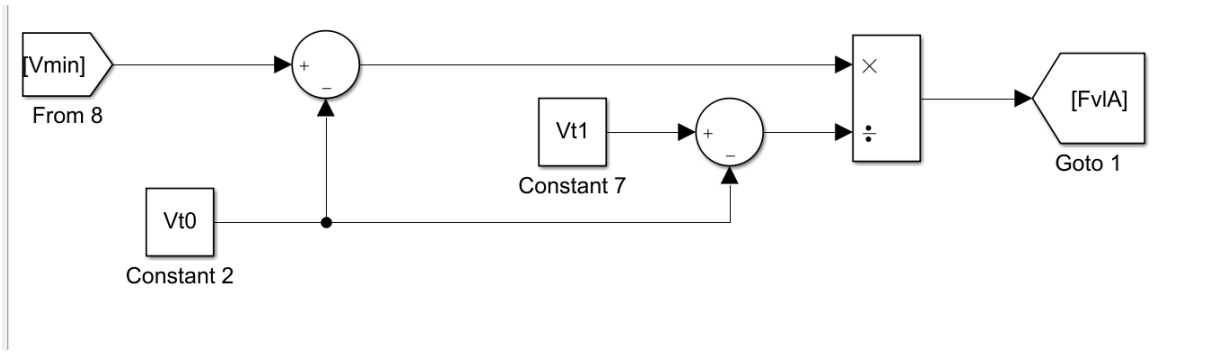

Figure 3.28 *Simulink representation of the low voltage tripping flag value while decreasing between Vt1 and Vt0*

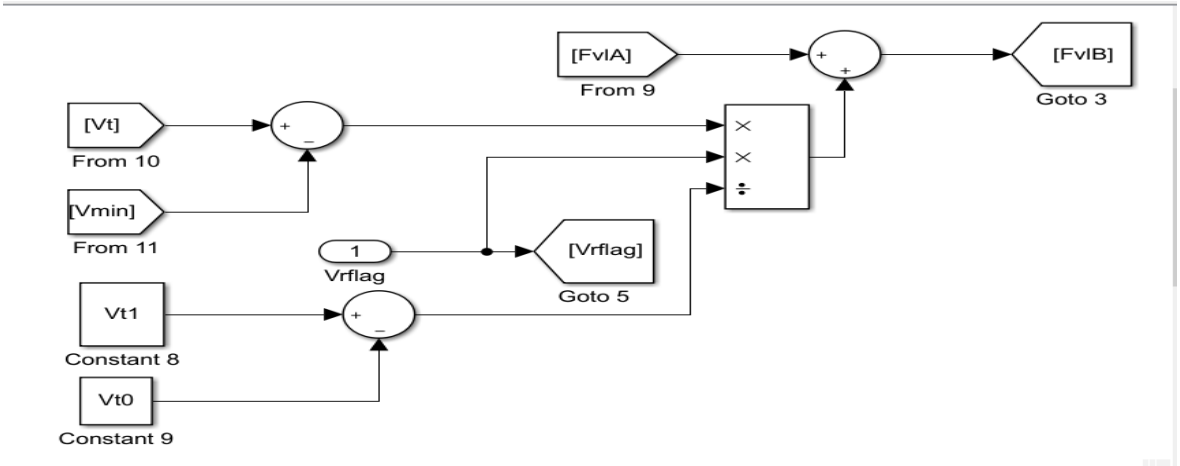

Figure 3.29 *Simulink representation of the partial reconnection low voltage tripping flag value while recovering above Vmin.*

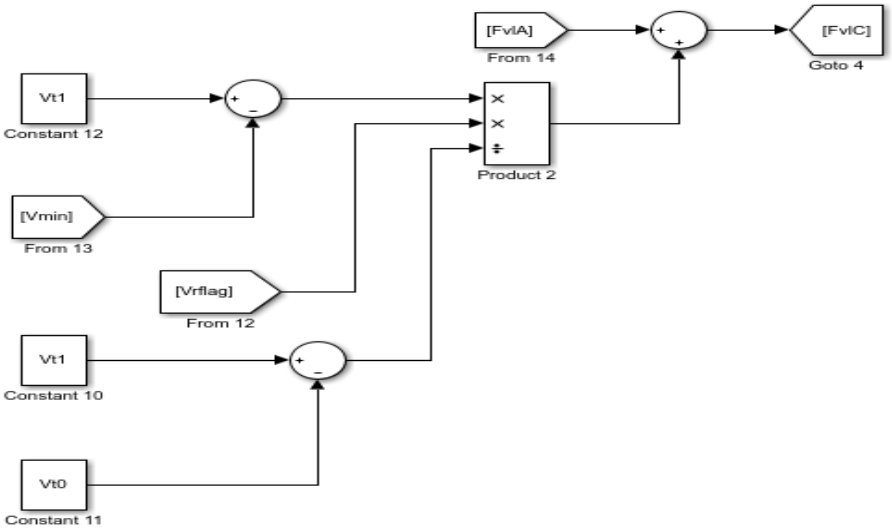

Figure 3.30 *Simulink representation of low voltage tripping flag value when Vt has been below Vt1 but has recovered*

High Voltage Tripping Flags:

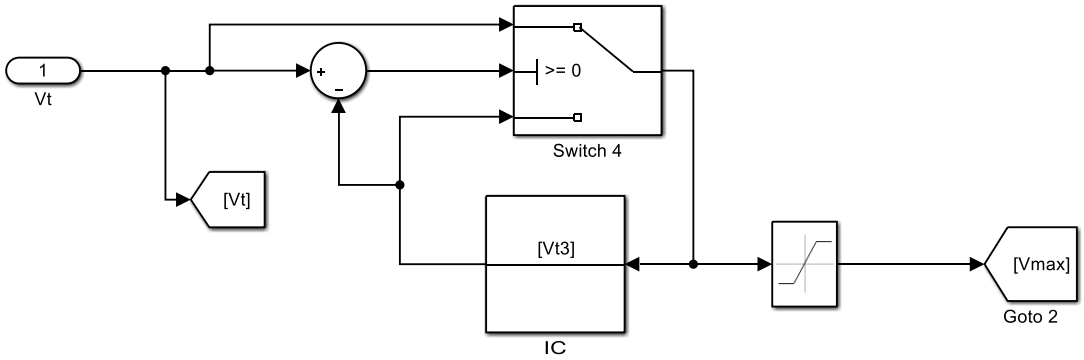

Figure 3.31 *Simulink representation of the High voltage tripping, tracking highest voltage* V_{max}

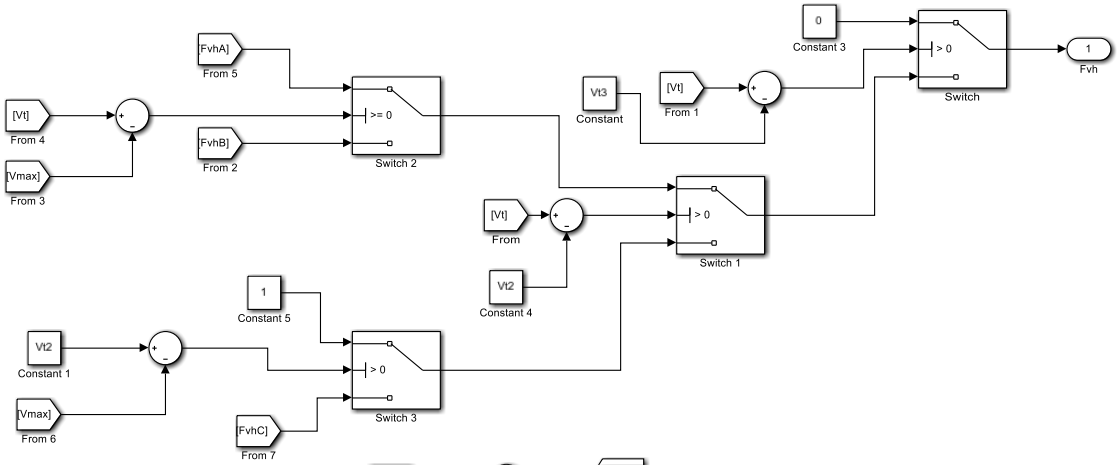

Figure 3.32 *Simulink representation of the High Voltage tripping logic*

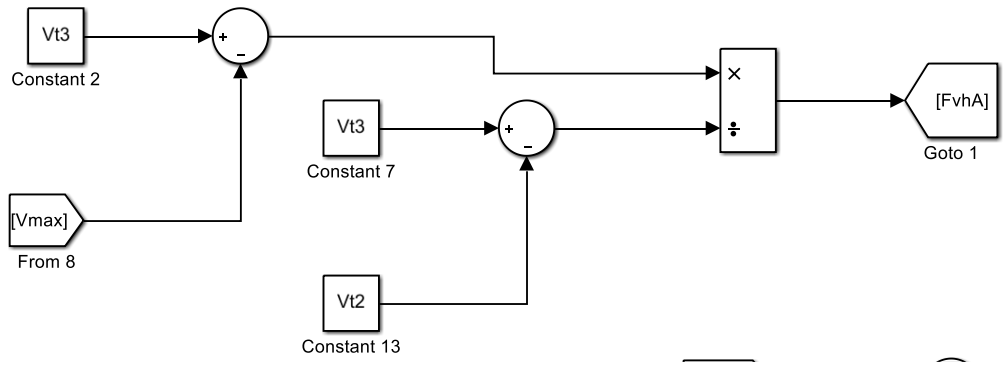

Figure 3.33 *Simulink representation of the high voltage tripping flag value while decreasing between Vt2 and Vt3*

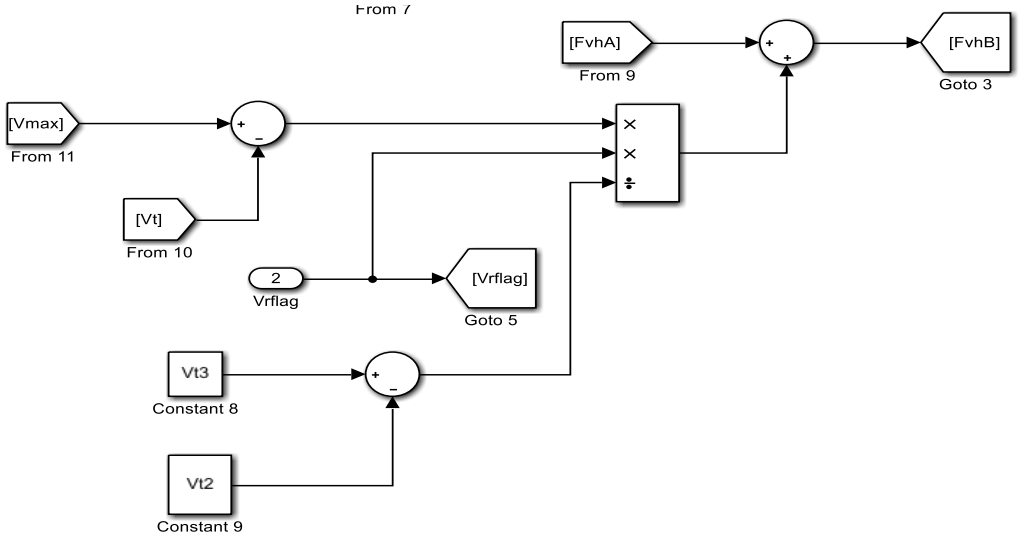

Figure 3.34 *Simulink representation of the partial reconnection high voltage tripping flag value while recovering above Vmax.*

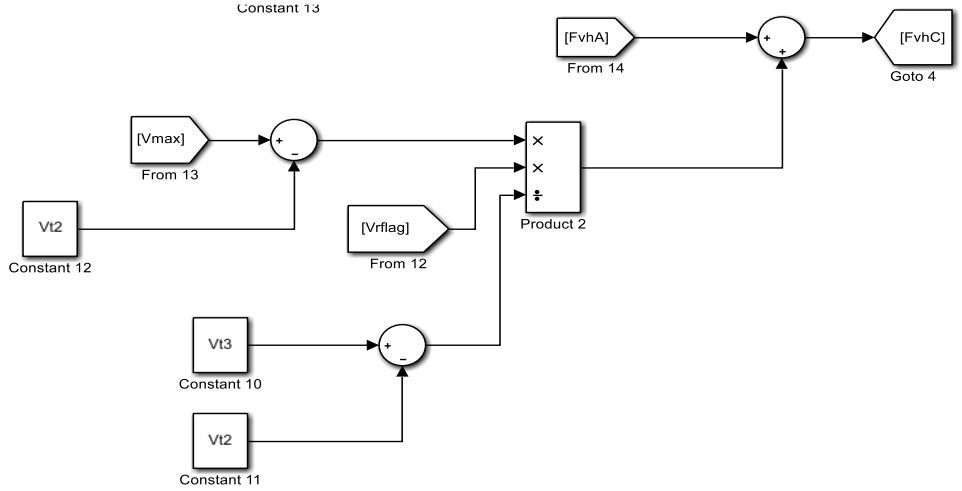

Figure 3.35 *Simulink representation of high voltage tripping flag value when Vt has been below Vt3 but has recovered*

Frequency Tripping Flags: The same as the low and high voltage tripping flags. This is done by changing the v to F. By combining Figure 3.26 to Figure 3.35, we get the complete tripping block subsystem as shown in Fig 3.36.

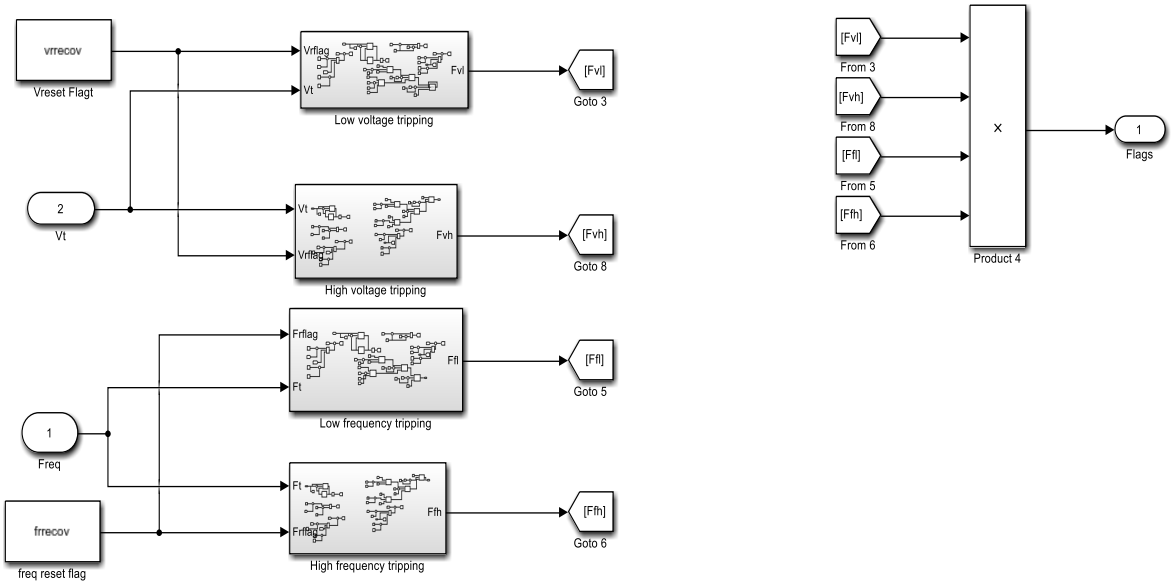

Figure 3.36 *Complete Simulink representation of Tripping Flags*

Subsystems: The subsystem block as shown in Fig 3.37 shows how the current is limited by saturation blocks to stay within permissible limits. The currents injected to the grid may be adjusted or reduced through the full or partial disconnection flags for low/high voltage/frequency events. The model also contains a delay block, which helps break any algebraic loops and also represents any delays from the power electronics.

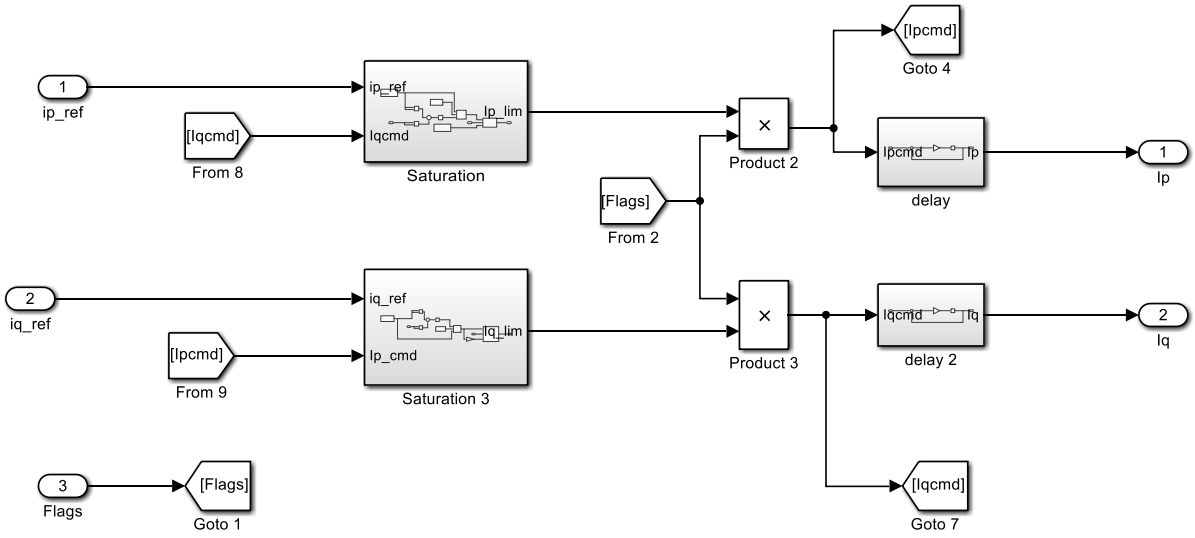

Figure 3.37 *Complete Simulink representation of the Subsystem Block*

The saturation blocks as shown in Figure 3.38 and Figure 3.39 show the apparent current limit for the reactive and active currents.

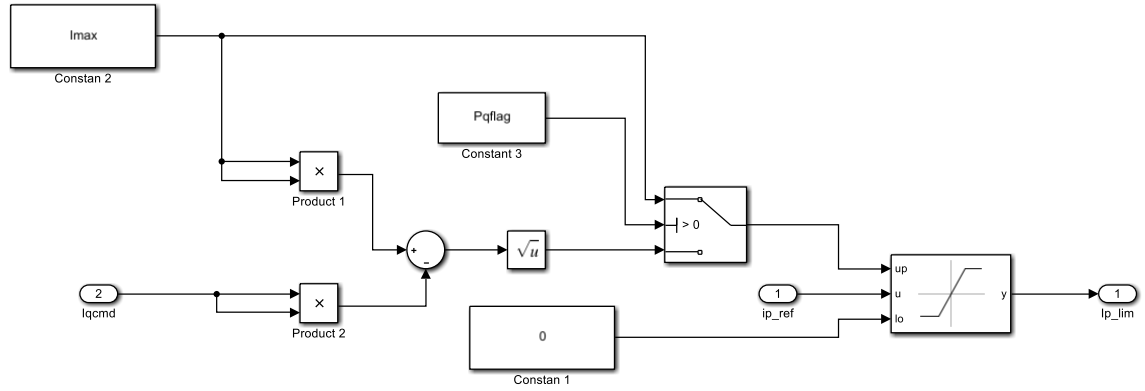

Figure 3.38 *Simulink representation of the apparent current Limit for active current*

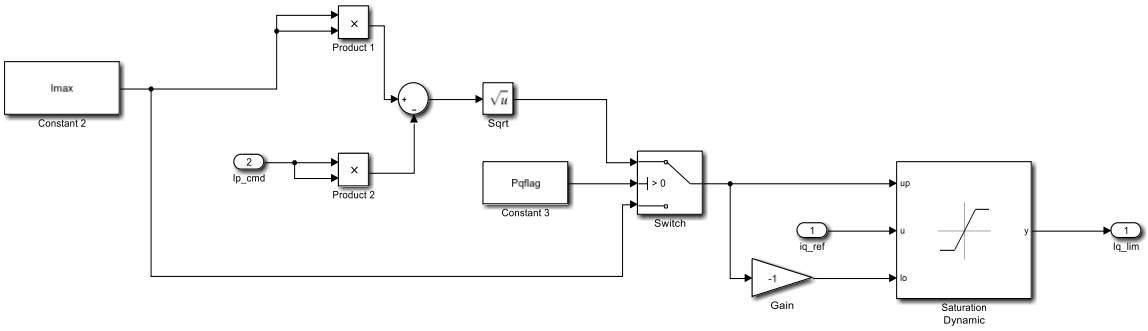

Figure 3.39 *Simulink representation of the apparent current Limit for reactive current*

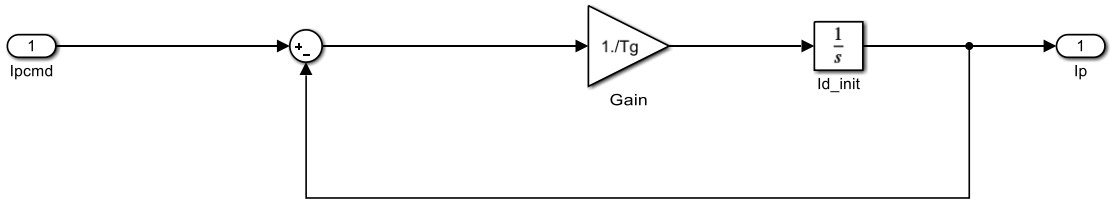

Figure 3.40 *Simulink representation of the active current delay*

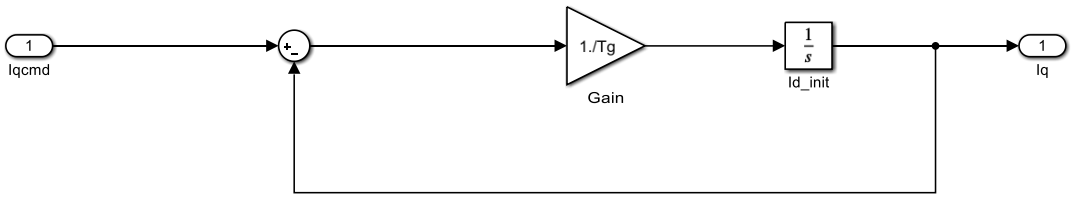

Figure 3.41 *Simulink representation of the reactive current delay*

System Reference:

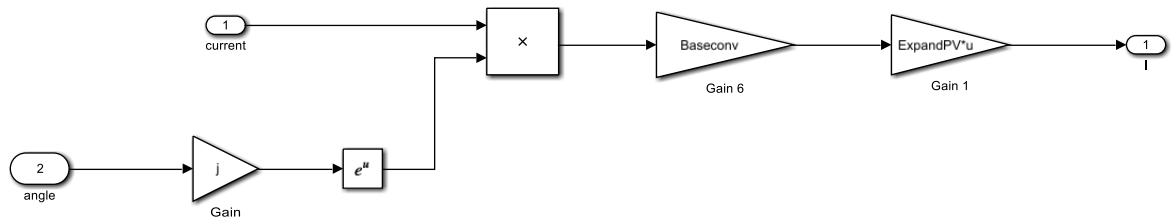

Figure 3.42 *Simulink representation of the system reference block*

Putting together all the blocks together gives the complete Simulink representation of the Photovoltaic model as shown in Figure 3.43

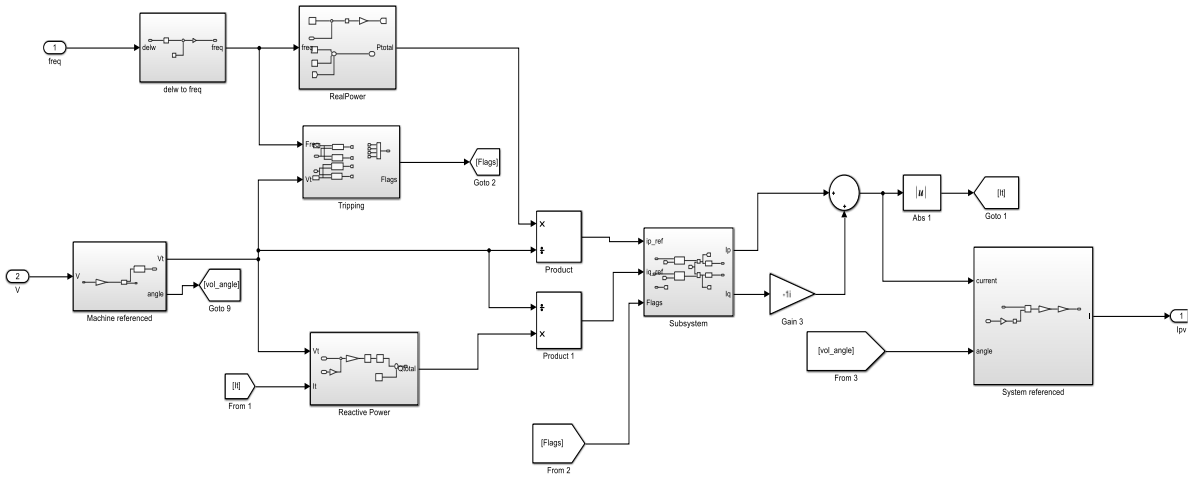

Figure 3.43 *Simulink representation of the complete PV Model*

NETWORK OF THE SMIB AND PV MODEL

Assuming V_b, Z_{net} and I_b is a vector (7 x 1) of bus voltages as seen in Chapter Four (Figure 4.12), impedance matrix (7 x 7), and vector (7 x 1) of current injection at the buses, then V_b can represented as in Equation 17

$$V_b = Z_{net} I_b \tag{17}$$

$$\begin{bmatrix} V_1 \\ V_2 \\ V_3 \\ \vdots \\ \vdots \\ V_6 \\ V_7 \end{bmatrix}_1 = \begin{bmatrix} Z_{1,1} & \cdots & Z_{1,6} & Z_{1,7} \\ Z_{2,1} & \cdots & Z_{2,6} & Z_{2,7} \\ \vdots & \vdots & \vdots & \vdots \\ \vdots & \vdots & \vdots & \vdots \\ Z_{6,1} & \cdots & Z_{6,6} & Z_{6,7} \\ Z_{7,1} & \cdots & Z_{7,6} & Z_{7,7} \end{bmatrix} \begin{bmatrix} I_1 \\ I_2 \\ \vdots \\ \vdots \\ I_6 \\ I_7 \end{bmatrix} \tag{18}$$

Where the current injection at bus 2 is from the SMIB while bus 6 is from PV. There are no current injections at 1, 3, 4 and 5. Bus 7 is the infinite bus, the current injection (I_7) at bus 7 is unknown, but the voltage is known. Hence Equation can 18 be rewritten as in Equation 19:

$$\begin{bmatrix} V_b \\ V_7 \end{bmatrix} = \begin{bmatrix} Z_A & Z_B \\ Z_C & Z_D \end{bmatrix} \begin{bmatrix} I_B \\ I_7 \end{bmatrix} \tag{19}$$

From Equation 19, Equation 20 is deduced

$$I_7 = Z^{-1}{}_D (V_7 - Z_C I_b) \tag{20}$$

The voltage is given in Equation 21 while the Simulink representation is shown in Figure 3.45

$$V_b = (Z_A - Z_B Z^{-1}{}_D Z_c) I_b + Z_B Z^{-1}{}_D V_7 \tag{21}$$

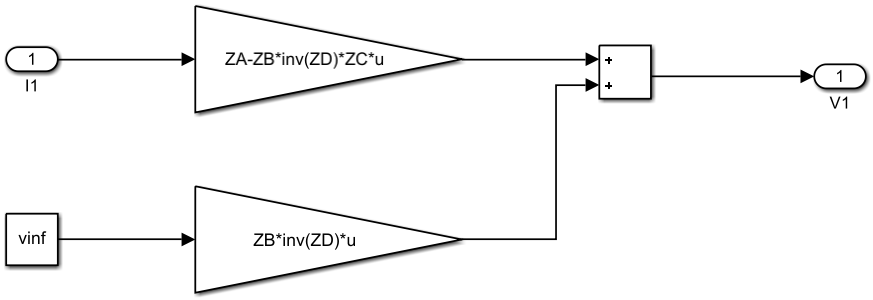

Figure 3.44 *Simulink representation of the SMIB-PV Network*

3.3.1.4 SMIB AND PV INTEGRATED INTO THE NETWORK

The SMIB system in Figure 3.19 and the PV model in Figure 3.44 is connected into one system with the network block above to form the complete system shown in Figure 3.46 The selector block (Smachs, PVmachs) specifies the bus number.

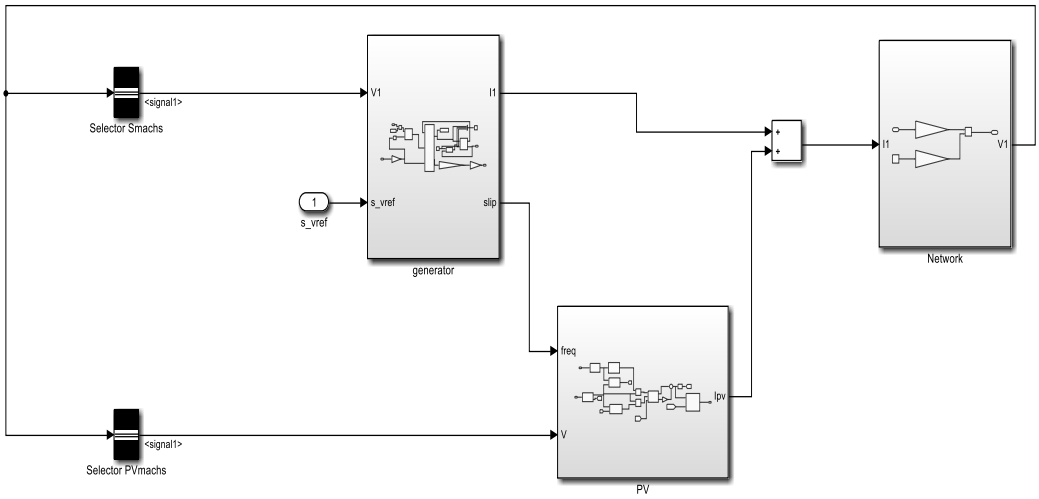

Figure 3.45 *Complete SMIB-PV Model with Network Connected*

3.3.1.5 SMIB AND PV INTEGRATED WITH PSS

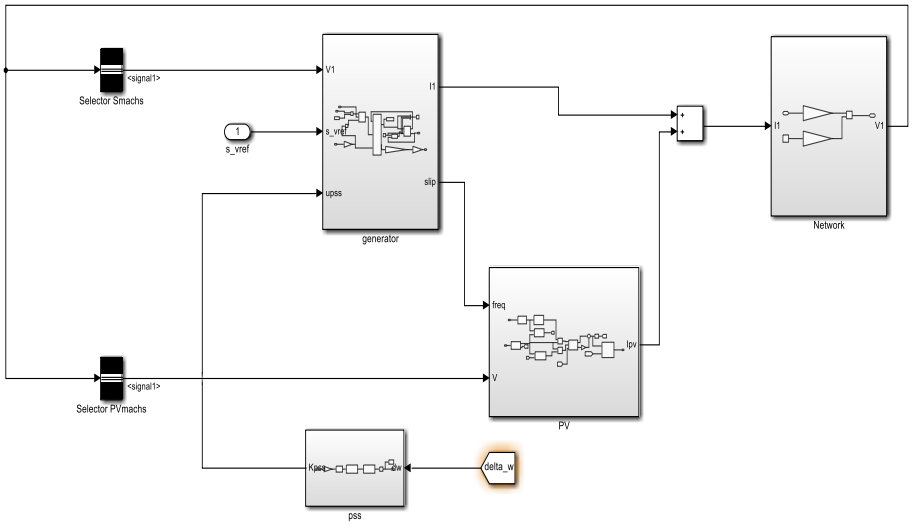

Figure 3. 46 *Complete SMIB-PV Model with Network and PSS integrated*

The completed SMIB-PV system in Figure 3.46 is integrated with the power system stabiliser (PSS) which is connected with the generator block as placed in Figure 3.47. The selector block (Smachs, PVmachs) specifies the bus number. Simulation results are placed in Chapter 4.

3.4 DESIGN OF THE POWER SYSTEM STABILISER

This research makes use of the conventional lead-lag PSS connected to the excitation system IEEE-ST1-type for analysis [40], The ith system transfer function in Equation (22) describes the PSS connection with IEEE-ST1 excitation system as follows[43].

$$G_i(s) = \frac{V_{pssi}(s)}{\Delta\omega_i(s)} = K_{pssi}\frac{T_\omega(s)}{(1+sT_\omega)}\frac{1+sT_i}{(1+sT_{2i})}\frac{1+sT_{3i}}{(1+sT_{4i})} \quad (22)$$

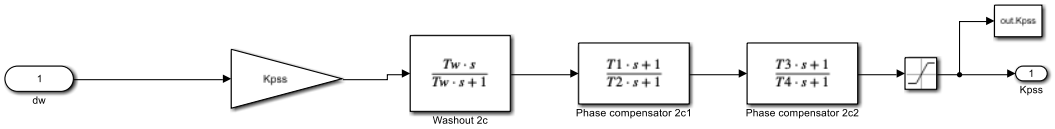

Figure 3.47 *Conventional Lead-Lag PSS*

Where the output signal of the PSS at the i_{th} machine is V_{PSSi}, Tw is the washout time constant equal to 10 in this study, the ith machine synchronous speed deviation signal is Δw_i. Optimal parameter of stabilizer gain K_{pssi} and parameters T_{1i}, T_2 , T_{3i}, and T_{4i} , are to be determined.

3.4.2 Transit Search Optimization Algorithm

The literature review in chapter two introduces the Transit search (TS) Optimisation Algorithm as novel astrophysics inspired metaheuristic algorithm based on exploration of exoplanets. Here, the mathematical modelling and application of the algorithm on the PSS are explained. The transit search method is used in discovering habitable exoplanets which are planets that are outside the solar system and orbit a star other than the sun.

So far, many planets have been discovered however, identifying planets alone is not important, the most important challenge is to find planets that can host life. There are five phases for implementing the TS algorithm, they are: the Galaxy phase, Transit phase, Planet phase, Neighbour phase and the Exploitation phase.

Galaxy phase: The purpose of this phase is to select the appropriate situations to perform the main stages of the algorithm (phases 2 to 5). This phase is performed only once before starting the iterations. The first thing is to identify habitable zones, the galaxy. To do this, n_s*SN random regions L_R are evaluated using Equation 23 to 26 to find the positions with the best stellar region with the most probability to host life.

$$L_{R,l} = L_{Galaxy} + D - Noise \qquad l = 1, \dots\dots\dots n_s xSN \quad 23$$

In which,

$$D = \begin{cases} c_1 L_{galaxy} - L_r & if\ z = 1(Negative\ Region) \\ c_1 L_{galaxy} + L_r & if\ z = 2(Positive\ Region) \end{cases} \quad 24$$

$$Noise = (c_2)^3 L_3 \quad 25$$

$$L_{s,i} = L_{R,i} + D - Noise \qquad i = 1, \dots\dots\dots n_s \quad 26$$

In the equations mentioned above, L_{Galaxy} represents the centre location of the galaxy. Also, L_r is a random location in the search space. There are two coefficients between 0 to 1 which indicate a random number ($c1$) and a random vector ($c2$) with the size of the number of variables for the optimization problem. In the next step, from each of the selected regions, a star, which is corresponded to a stellar system, must be chosen.

Transit Phase: In order to detect the transit, it is necessary to re-measure the amount of light received from the star to detect its possible reduction in the received light signals. The luminosity of a star (or absolute brightness) is its intrinsic brightness, which deals with the amount of energy that a star radiates per second. Besides this, the apparent brightness of the star is how bright it appears to the observers. The luminosity of a star can be estimated based on the spectrum of light (star class) received by the observer (telescope) and the distance of the star from the observer. It is clear that the small distance causes to receive more photons. Accordingly, in the proposed algorithm, the luminosity of the star is obtained approximately from Equation (27)

$$L_i = \frac{R_i/n_s}{(d_i)^2} \qquad i = 1, \dots\dots\dots n_s \qquad R_i \epsilon \{1, \dots\dots, n_s\} \quad 27$$

$$d_i = \sqrt{(L_S - L_T)^2} \qquad i = 1, \dots\dots\dots\dots, n_s \quad 28$$

$$if\ Li_{new} < L_i \quad P_T = 1(Transit)$$
$$if\ Li_{new} \geq L_i \quad P_T = 0\ (No\ Transit) \quad 29$$

In which, L_i and R_i are the luminosity and rank of the star i. Also, di (Eq. (28)) deals with the distance between the telescope and the star i. The location of the telescope, L_T, is selected randomly at the start of the algorithm and does not change during optimization. This probability, PT, denoted by 1 (probability of transit) and zero (non-transit), is specified as based on Eq. (29). If PT = 1, the planet phase is used, otherwise, the neighbour phase is implemented in the current iteration.

Planet Phase: By specifying the value of P_T in the previous phase, if the transit is observed (PT = 1), the planet phase is implemented in the TS algorithm. In this phase, first, the initial location of the detected planet is determined. Given that the light received by the observer (telescope) is received from the star, so a decrease in the amount of this light (occurrence of transits) occurs when the planet has passed between the star and the telescope. Based on this, the initial location of the detected planet (Lz) can be determined. In the TS algorithm, this is done by Eq. (30).

$$L_z = {(c_8 L_T + R_l L_{si})}/{2} \qquad \text{i= 1.....} n_s \qquad 30$$

In which,

$$R_L = {L_{snew,i}}/{L_{s,i}} \qquad 31$$

The parameter R_L represents the luminance ratio as calculated by equation (31). The coefficient $c8$ also has a random value between 0 and 1. In equation 31, using the average of the two relative locations of the star and the telescope, the situation of the planet whose current location is between the star and the telescope is determined. In each iteration of the algorithm, if the detected planet is better than the previously discovered planet in the stellar system under study (better conditions for life), the location of this planet is saved. Therefore, in the TS algorithm, there is only one planet (the best planet) for each n_s star.

Neighbour Phase: If there is no transit for a star in the current observation, the neighbourhood planets of the previously detected planet for the star will be studied. In other words, if the neighbour has better conditions than the current planet (it has better conditions to host life), it will be replaced with the current planet of the star. This is done in the TS algorithm in the neighbour phase using equations (31) to (33). First, the initial location of the neighbour (Lz) is estimated using equation (33) with consideration of its host star (LS, new) and a random location (LR). Then, the final location of the neighbour planet (LN) is determined by equations (34) and (35). The coefficients $c11$ and $c12$ in Eq. (33) deal with a random number between 0 and 1.

$$L_p = \frac{\sum_{J=1}^{SN} L_{mj}}{SN} \qquad 32$$

$$L_z = {\left(c_{11} L_{s,new} + c_{12} L_r\right)}/{2} \qquad 33$$

$$L_{n,j} = \begin{Bmatrix} L_z - c_{13}\, L_r & if\ z = 1(Negative\ Region) \\ L_z + c_{13} L_r & if\ z = 2(Positive\ Region) \\ L_z + c_{14} L_r & if\ z = 3 \end{Bmatrix} \qquad 34$$

$$L_{N,i} = \frac{\sum_{J=1}^{SN} L_{nj}}{SN} \qquad 35$$

Exploitation Phase: The aim from the previous phases is to discover the best planet for each star. As mentioned earlier, discovering a planet alone does not matter as a major constraint is to study the characteristics of the planet and the conditions to host life. In the TS algorithm, this is done in the Exploitation phase. In this phase, L_P in the current phase (L) refers to the characteristics of the planet (such as its density, materials, atmosphere, etc.). Then, by adding new knowledge (K), the final characteristics of the planet are modified SN times (j = 1,. . . , SN) using equations (36) and (37). In this equation, c_{15} is a random number between 0 and 2, and c_{16} is a random number between 0 and 1. Also, c_{17} is a random vector between 0 and 1.

$$L_{E,j} = \begin{Bmatrix} c_{16} L_p + c_{15} K & if\ c_k = 1 & (State\ 1) \\ c_{16} L_p - c_{15} K & if\ c_k = 2 & (State\ 2) \\ L_p - c_{15} K & if\ c_k = 3 & (State\ 3) \\ L_p + c_{15} K & if\ c_k = 4 & (State\ 4) \end{Bmatrix} \qquad 36$$

$$K = (c_{17})^P L_r \qquad 37$$

To better express the implementation process of the TS algorithm for the optimal tuning of the PSS, the following steps are presented:

1. Initialise from a random galaxy and determine the habitat zone by imputing the number of host stars(n_s) and Signal to Noise Ratio (SN). where n_s*SN = Population size. Input the number of iterations. The best solution is expressed by the best $n_{s,i}$ planet for each star and is described as i = {K_{pss}, T_1, T_2, T_3,T_4,T_5} in the PSS controller.
2. Run to obtain the best planet L_B and the fitness function f_b using the objection function equation in eq.
3. Initialization of the galaxy phase using equation 23 - 26 and return with the location of the best stars Ls.

4. To confirm the transit, luminosity of the star is observed to obtain Li using the location of the telescope Lt and distance from observer to the star di as in equation 27 and 28. If any transit is detected for i=1:$n_{s,}$ move to the planet phase using equation 29 to obtain P_T else, go to the Neighbour phase. New location $L_{s,new}$ is obtained in a region i.
5. The initial location (Lz) of the planet detected in the transit phase by luminosity is then obtained in the planet phase. This is obtained from equation 30.
6. If no transit is observed in the transit phase, the neighbour phase is initialised using equation 33 and 35 to obtain final location of the best planet L_N.
7. The characteristics of the planets is conducted in the exploitation phase iterating j= 1,.....SN. using equation 36 and 37. The best planet for each star is obtained as the L_E in this phase.

In this research, Genetic Algorithm (GA) and Particle Swarm Optimization (PSO) was adopted to validate the proposed Transit Search Optimization (TS) algorithm in PSS design. This was done by comparing their performances based on obtained results in chapter four. As the study in [41] notes, of all the meta-heuristic algorithms, GA and PSO have most widely been used for designing PSS. The procedure for GA and PSO is elucidated below.

Particle swarm optimization: The mathematical formulation and explanation of PSO can be seen in the study [42], the steps for PSO application to PSS design are explained below;

The steps of the PSO algorithm for optimal PSS tuning are as follows.

1. Initialize population size, the vector $x = [KPss, T1, T2, T3, T4]$ is the PSS controller parameters.
2. Specify parameters of PSO which include inertia coefficient (w), personal acceleration coefficient ($c1$), social acceleration coefficient ($c2$).
3. Initialize particle position, and velocity, evaluate the objective function, and global best.
4. Iteration loop, update position, velocity, update global best and evaluate the objective function
5. Go to step 3, if maximum iteration is not reached otherwise end.

The flowchart of these steps is shown below.

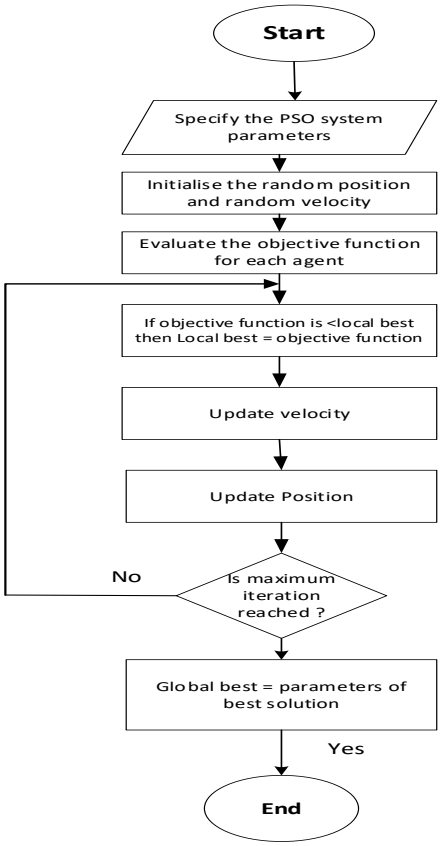

Figure 3.48 Flowchart of Particle swarm optimization algorithm

Genetic Algorithm: The mathematical formulation and explanation of GA can be seen in the study [44], the steps for GA application to PSS design are explained below;

The steps of the GA algorithm for optimal PSS tuning are as follows.

1. Initialize population, the vector $x = [KPss, T1, T2, T3, T4]$ is the PSS controller parameters.
2. Select parents and perform crossover.

3. Perform mutation operation (mutate off-springs from parents).
4. Merge main population and off-springs.
5. Evaluate, sort, and select new population
6. Go to step 2, if maximum iteration is not reached, and repeat the evolution loop otherwise end.

System Linearization:

The power system is made up of various dynamic elements and is modelled using differential algebraic equations (DAEs) as seen in the SMIB models. This power system DAEs are solved using ordinary differential equations (ODEs) solver in Matlab/Simulink IDE. However, PSS design adopts the linear control theory, hence, the power system model is linearized using the 'linmod' command in the Matlab command window. The linearized model is extracted from the non-linear power system model before the PSS damping controller can be designed. This section explains basic expressions for the linearization approach for differential equations (DE). The behaviour of a system can be represented by a first-order DAE in the following form as in equation 38[20]:

$$\begin{aligned} \frac{dy}{dx} &= f(x,z,u) \\ 0 &= g(x,z,u) \\ y &= h(x,z,u) \end{aligned} \qquad 38$$

Where f is the nonlinear DEs function that denotes the system controller dynamics, x is the system vector which involves generator angle, speed, flux, transient voltage, automated voltage regulator (AVR) output, excitation system, etc., z denotes the algebraic variables which include the system voltage angle and size, the stator currents, etc., u is the reference vector which involves excitation control reference voltage, mechanical input, and other input variables and y denotes the output vector with signals such as generator speed, line power, system voltage size. By linearizing Equations around an operating point, Equation 38 initial equilibrium is achieved as shown in equations 39 - 41.

$$\frac{d\triangle x}{dt} = \frac{\partial f}{\partial x}\Delta x + \frac{\partial f}{\partial z}\Delta z + \frac{\partial f}{\partial u}\Delta u \qquad 39$$

$$\Delta y = \frac{\partial h}{\partial x}\Delta x + \frac{\partial h}{\partial z}\Delta z + \frac{\partial h}{\partial u}\Delta u \qquad 40$$

$$0 = \frac{\partial g}{\partial x}\Delta x + \frac{\partial g}{\partial z}\Delta z + \frac{\partial g}{\partial u}\Delta u \qquad 41$$

If Δz is removed from the above equations, the state equation of the power system can be represented in equation 42 below:

$$\begin{aligned} \frac{d\triangle x}{dt} &= A\Delta x + B\Delta u \\ \Delta y &= C\Delta x + D\Delta u \end{aligned} \qquad 42$$

4.2 Objective Function Formulation

Rotor speed deviation error results in electromechanical modes of oscillation, to improve the damping of these electromechanical modes (EMs), is to minimize the rotor speed deviation error, through which the damping ratio is maximized for faster oscillation attenuation. The eigenvalue objective function was employed to enhance the damping characteristics of electromechanical modes (EMs) in the system and shift the eigenvalues of the power system to the left region of the complex s-plane. Stabilizer gain and parameters of the PSS are determined through the defined eigenvalue objective function as follows in Equation 43.

$$J = max\{real(\lambda_i)|\lambda_i \epsilon EMs\} + P_c \sum\{real(\lambda_j)|\lambda_j > 0\} \qquad 43$$

$$EMs = \left\{\lambda_k | 0 < \frac{im(\lambda_k)}{2\pi} < 5\right\}$$

The eigenvalues of the power system state space matrix are denoted by λi, P_C is a penalty constant applied in producing positive eigenvalues and can enhance slow eigenvalues [28]. In this study, P_C is considered to be 50. J, which is the objective function, is minimized subject to PSS gain ($Kpssi$) and parameters ($T1_i$, T_{2i}, T_{3i}, and T_{4i}) subject to the constraints $0.001 \leq Kpssi \leq 50$ and $0.001 \leq T_{1i} \leq 1$, $0.02 \leq T_{2i} \leq 1$, $0.001 \leq T_{3i} \leq 1$ and $0.02 \leq T_{4i} \leq 1$. The TS algorithm proposed for PSS design computes the defined optimization problem using the objective function and constraints to obtain optimal values.

4.1 Results and Discussion

The results obtained from the simulations conducted in Matlab/Simulink software in line with the methodology and objectives of this thesis. Above all is the simulation of the Transit Search (TS) optimisation algorithm and its performance evaluation on the test models.

4.3 Objective 1: Single Machine Infinite Bus (SMIB) Test System Simulation Results

The SMIB system modelled in chapter three is now used for numerical simulations. Figure 4.1, shows the single-line diagram while Table 4.1 and 4.2 show the bus and line data adopted from [26] respectively.

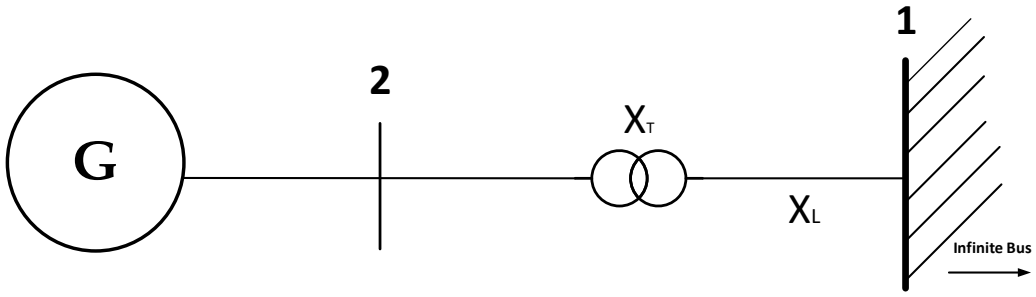

Figure 4.1 *Single Line Diagram of a SMIB*

Bus No.	Voltage	Angle	Pg	Qg	PL	QL	GL	BL	Bus type
1	1.026	0.00	0.00	0.00	0.00	0.00	0.00	0.00	1
2	1.025	0.00	2.50	0.00	0	0	0	0	2

Table 4.1 SMIB Bus data

From Bus	To Bus	R	X	B	Tap	Ratio
1	2	0.0000	0.2625	0.0000	1.00	0.00

Table 4.2 SMIB Line Data

The script "SMIB_run.m" in the appendix uses the functions "form_Ymatrix.m" and "power_flow.m" which takes the data from Tables 4.1 and 4.2 and outputs the Y admittance matrix result and also the bus and line flow solution shown below in Figure 4.2

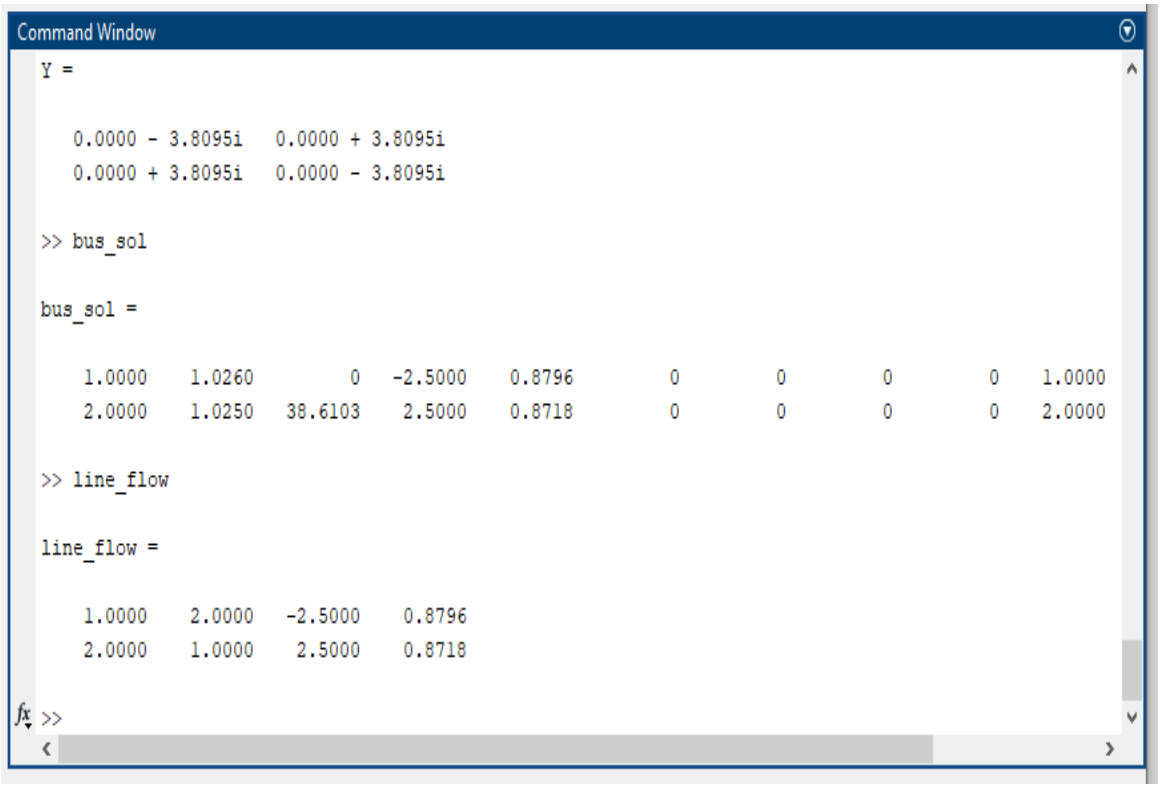

Figure 4.2 Y admittance matrix and power flow solution of the SMIB Model

The next stage will be to initialize the SMIB parameters using the script "SMIB_run.m" in the appendix. This initializes the SMIB parameters using the machine data "mac_con". It also requests for the scripts "Synch_parameter_gen_base.m" and "generic_Sync_Init.m" in its program. The former assigns values from the "mac_con" to the different variables of the synchronous machine modelled in chapter three while the latter computes the equations used for the synchronous machine modeled in chapter three. The concluding part of the

"SMIB_run.m" introduces a three-phase fault on the system by specifying a very large admittance at bus 1 where the generator is connected at 1 second. The uncontrolled generator rotor speed deviation and rotor angle are displayed in Figures 4.3 and 4.4 respectively.

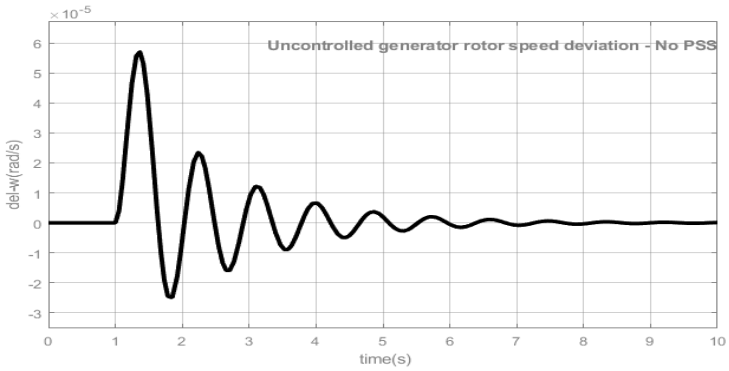

Figure 4.3 Uncontrolled generator rotor speed deviation

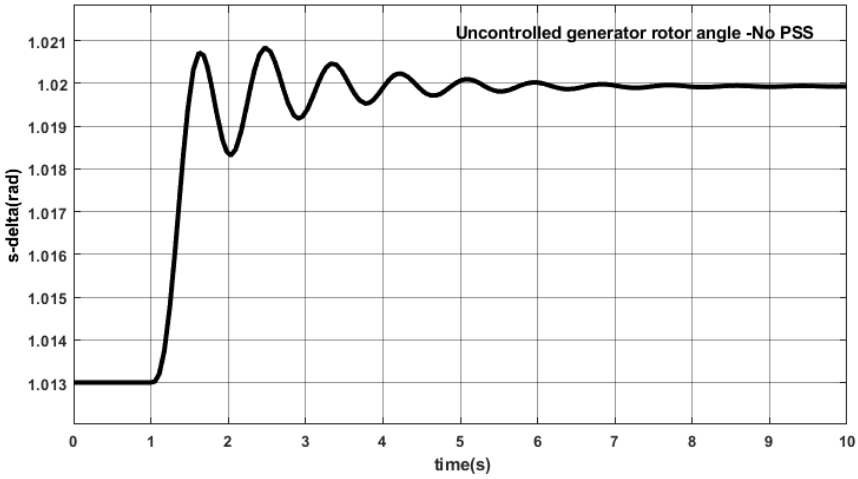

Figure 4.4 Uncontrolled generator rotor angle

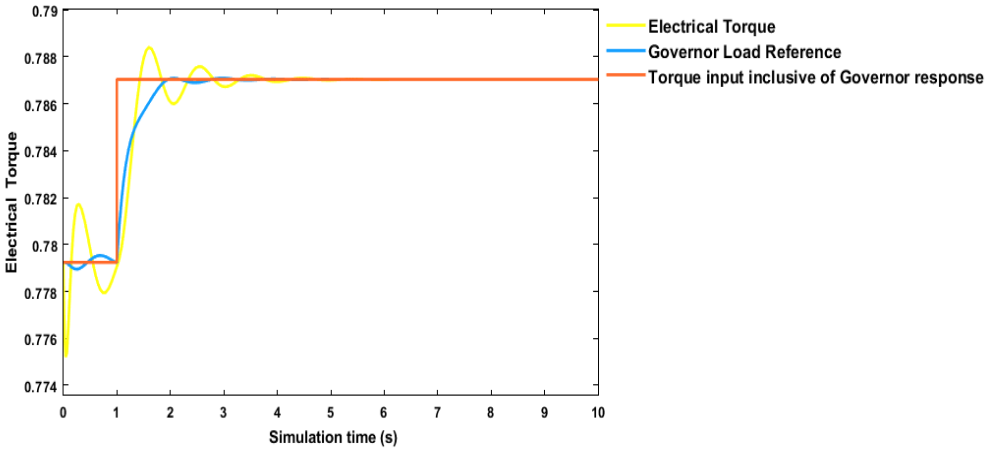

Figure 4.5 *Synchronous machine step response to change in governor load reference*

By using the [A, B, C, D] = linmod('casefile') command to linearize the system which in this case is the SMIB and [L] = eig(A), where A is the system matrix of the SMIB test model, the eigenvalues of the system in Matlab command window is obtained. This is displayed in Table 4.3 while Figure 4.6 shows the eigenvalues plot in the s-plane. As observed, all the eigenvalues from Figure 4.6 are seen shifting to the RHS of the s-plane which signifies that the system experienced some sort of instability.

NO -PSS		
Mode	**Eigenvalues**	**Damping Ratio**
1	0.7659 + 7.5917i	-0.1004
2	0.7659 – 7.5917i	-0.1004
3	-13.6250 + 0.0000i	1.000
4	-8.5260 + 0.0000i	1.000
5	-4.4711 + 0.0000i	1.000

Table 4.3 *Uncontrolled System Eigenvalue*

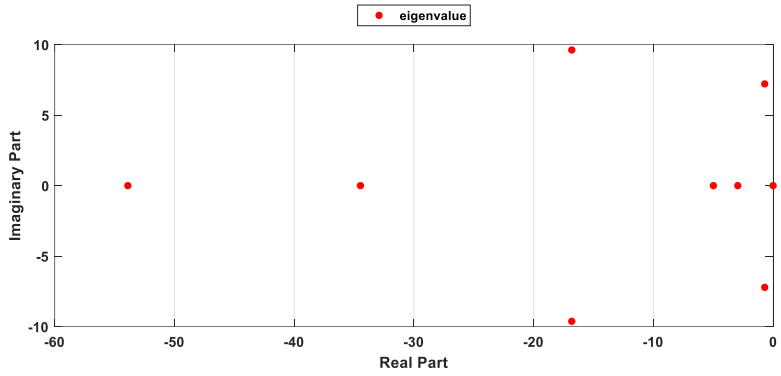

Figure 4.6 Uncontrolled system eigenvalue plot

From Table 4.3, the damping ratios of each corresponding Modes are depicted.

4.3 SMIB Integrated with PSS

In order to design the Power System Stabiliser (PSS) to control the generator rotor speed deviation and rotor angle, the eigenvalue objective function discussed in chapter three is implemented, and the TS, PSO and GA optimization programs in the appendix are then used to obtain the optimized PSS parameters in Table 4.4. The PSS design convergence rate curve comparing TS, GA, and PSO in Figure 4.7, the curve shows which optimization technique converged faster in optimal PSS design. From Figure 4.7, TS converged at iteration 22, PSO at iteration 40, and GA at iteration 32. Thus, TS converged fastest of all the three algorithms.

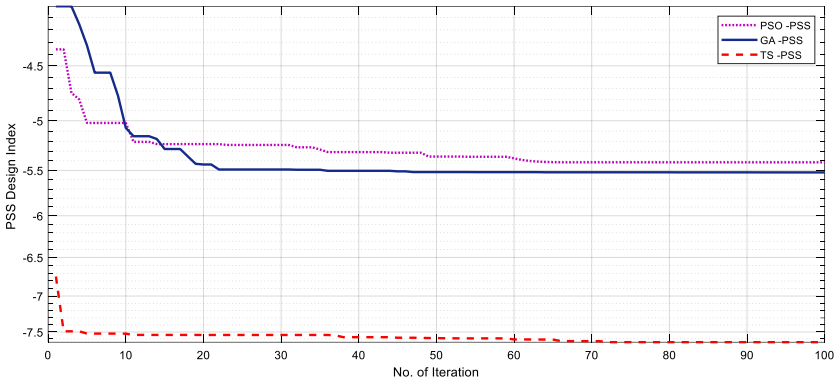

Figure 4.7 *PSS design convergence rate comparing GA-PSS, PSO-PSS and TS-PSS*

Algorithm	Kpss	T1	T2	T3	T4
PSO	97.1965	0.5810	0.0200	0.0692	0.6912
GA	34.2412	0.1682	0.6385	0.5043	0.0791
TS	99.9633	0.0689	0.6274	0.6422	0.0200

Table 4.4 *PSS Optimal parameters using GA, PSO and TS Algorithm*

The PSS parameters from Table 4.4 are then used for simulation to control the generator rotor speed and generator rotor angle. Each algorithm performance is compared against each other, Figures 4.7 and 4.8 shows the performances for NO-PSS, GA-PSS, PSO-PSS, and TS- PSS respectively.

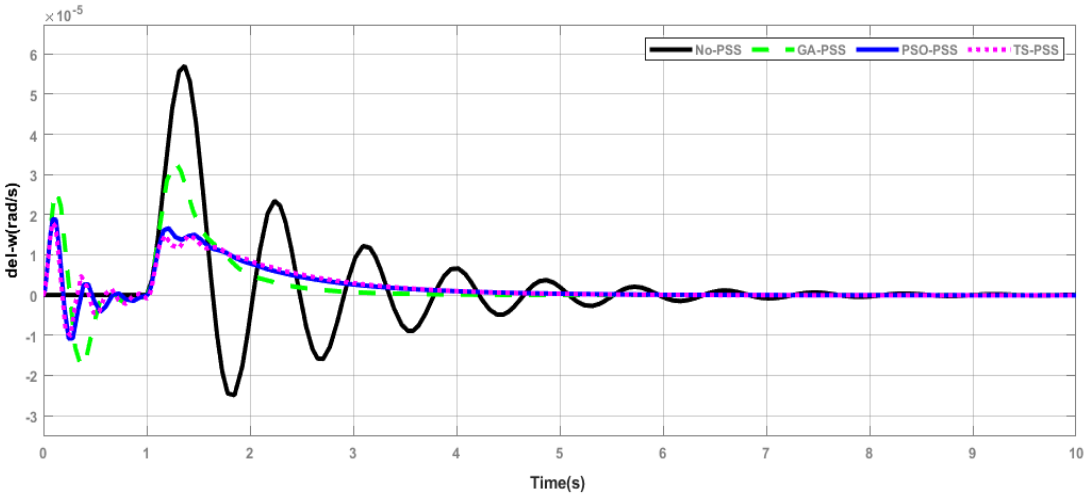

Figure 4.8 Controlled rotor speed deviation

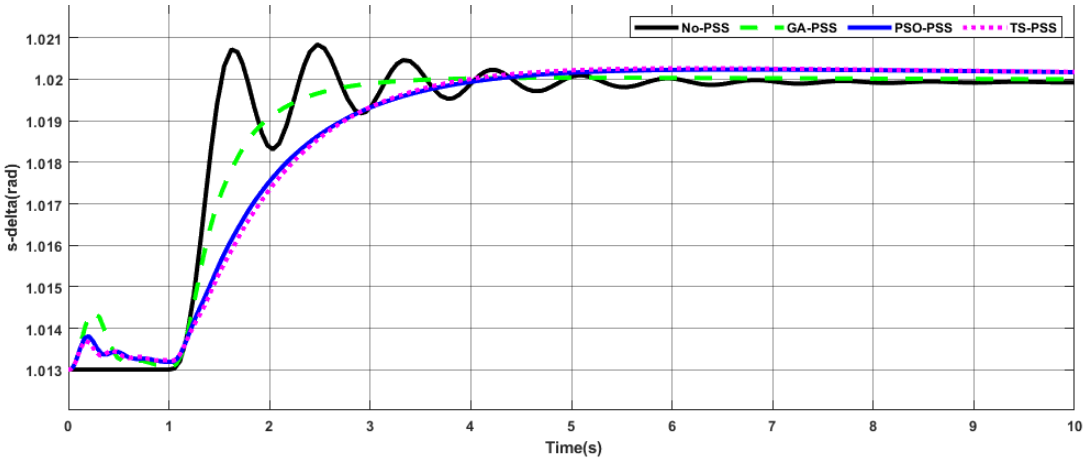

***Figure 4.9** Controlled generator rotor angle*

Also, the performance index from the simulation results above which compares the TS algorithm with GA and PSO as well as NO-PSS controller in terms of rise time, settling time and overshoot for the generator rotor speed deviation and rotor angle is shown in Table 4.5.

***Table 4.5** SMIB Test Performance Index*

	SMIB Transient Response											
	Settling Time (sec)				Rise Time (secs)				Overshoot			
	NO-PSS X 10^{-1}	GA-PSS X10^{-1}	PSO-PSS X 10^{-1}	TS-PSS X 10^{-1}	NO-PSS X 10^{-5}	GA-PSS X 10^{-5}	PSO-PSS X 10^{-5}	TS-PSS X 10^{-5}	NO-PSS X 10^{-5}	GA-PSS X 10^{-5}	PSO-PSS X 10^{-5}	TS-PSS X 10^{-5}
del ω	30.4561	18.8475	19.8457	15.8475	0.9543	0.0800	0.0800	0.0600	30.8059	25.8065	25.8065	25.8065
s_delta	31.0371	19.8475	18.8775	13.2245	0.9543	0.0800	0.0800	0.0600	30.8059	25.8065	25.8065	25.8065

Table 4.6 SMIB Improvement Index of the TS over the PSO and GA

	% Improvement Rotor angle Rotor speed (del ω)		% Improvement Rotor angle (s_delta)	
	TS vs GA	TS vs PSO	TS vs GA	TS vs PSO
Settling Time (sec)	15.92%	20.15%	33.4%	30%
Rise time (sec)	25%	25%	25%	25%

From Table 4.5, $delω$ the generator rotor speed deviation for the No-PSS controller in the system has a settling time of 3 seconds out of 10 which is the simulation time. GA-PSS settles at 1.88 seconds, PSO-PSS at 1.9 seconds and TS-PSS at 1.5 seconds. Also, for the generator rotor angle s_delta, when there was No-PSS controller in the system, the recorded settling time was 3.1seconds, with 1.9 seconds for the GA-PSS controller, 1.88seconds for PSO-PSS controller and 1.3 seconds for TS-PSS controller.

In the new operating condition of the SMIB test power system, eigenvalues with PSS controller installed in the system is shown in Table 4.3 with Mode 1 for the No PSS case condition, following an optimal PSS design, Mode 1 was enhanced from 0.7659 + 7.5917i to stable mode of -54.5768 + 0.0000i for TS-PSS, -22.4991 + 0.0000i for GA-PSS and -53.7700 + 0.0000i for PSO-PSS respectively as shown in Table 4.7 below.

Table 4.7 *SMIB power system eigenvalues for the electromechanical modes for GA, PSO and TS- PSS*

Mode	PSO-PSS	GA-PSS	TS-PSS
1	-53.7700 + 0.0000i	-22.4991 + 0.0000i	-54.5768 + 0.0000i
2	-0.2269 +15.0868i	-0.1202 +11.1775i	-0.0842 +16.4613i
3	-0.2269 -15.0868i	-0.1202 -11.1775i	-0.0842 -16.4613i
4	-14.2069 + 0.0000i	-0.1019 + 0.0000i	-14.2916 + 0.0000i
5	-4.6410 + 0.0000i	-1.4348 + 0.0000i	-0.1060 + 0.0000i
6	-0.1059 + 0.0000i	-5.3726 + 2.0984i	-1.5102 + 0.2160i
7	-2.3882 + 0.0000i	-5.3726 - 2.0984i	-1.5102 - 0.2160i
8	-1.0714 + 0.0000i	-4.3773 + 0.0000i	-4.6210 + 0.0000i

4.4 SMIB Integrated with PV

The integrated SMIB with PV system modelled in chapter three is now used for numerical simulations, Figure 4.9 shows the single line diagram. The bus and line data were formulated and as are shown in Tables 4.8 and Table 4.9.

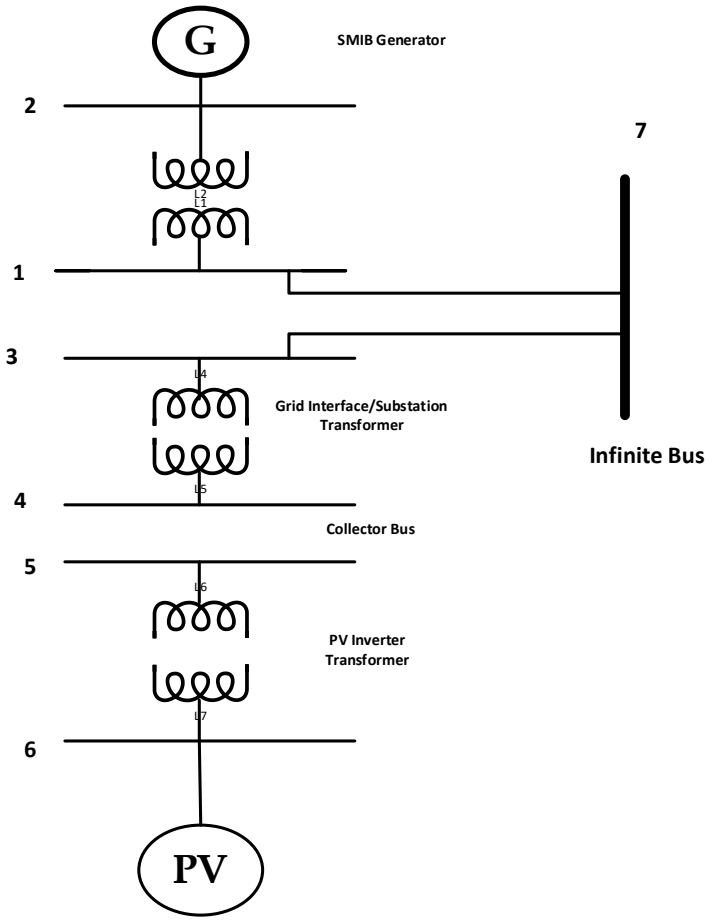

Figure 4.9 *Single line diagram of SMIB integrated with PV Generator*

Table 4.8 *SMIB and PV Bus Data*

	Voltage	Angle	Pg	Qg	PL	QL	GL	BL	Bus Type
1	1.00	0.00	0.00	0.00	0.00	0.00	0.00	0.00	3
2	1.025	0.00	2.50	0.00	0.00	0.00	0.00	0.00	2
3	1.00	0.00	0.00	0.00	0.00	0.00	0.00	0.00	3
4	1.00	0.00	0.00	0.00	0.00	0.00	0.00	0.00	3
5	1.00	0.00	0.00	0.00	0.00	0.00	0.00	0.00	3
6	1.00	0.00	2.00	0.125	0.00	0.00	0.00	0.00	2
7	1.040	0.00	0.00	0.00	0.00	0.00	0.00	0.00	1

Table 4.9 SMIB & PV Line data

From Bus	To Bus	R	X	B	Tap	Ratio
01	02	0.0625	0.2000	0.0000	1.0000	0.0000
01	07	0.1100	0.1000	0.0000	1.0000	0.0000
03	07	0.0100	0.1000	0.0000	1.0000	0.0000
03	04	0.0000	0.0500	0.0000	1.0000	0.0000
04	05	0.0075	0.0125	0.0200	1.0000	0.0000
05	06	0.0000	0.0250	0.0000	1.0000	0.0000

As seen in Figure 4.9 the single line diagram of the SMIB and PV integrated is a 7 Bus system. The same procedure for the SMIB test system is now implemented here on the PV integrated system, however, the difference is that the bus and line data changes as seen in Tables 4.8 and 4.9. the "script for the integrated SMIB and PV" uses the new bus and line data to calculate the Y admittance matrix and power flow. It also calls the "SMIB_run.m" and "powerflow4PV_smib", these two initialize the SMIB and PV parameters respectively. The concluding part of the powerflow4PV_SMIB introduces a 10000A three-phase fault on the system by specifying a very large admittance at bus 2 where the generator is connected at 1 second. The fault is initiated at 1sec and ends at 1.2sec. The uncontrolled generator rotor speed deviation is displayed in Figures 4.10 while Fig 4.12 shows the generator rotor angle deviation of the SMIB with Solar PV with no pss, Solar PV and the simulated fault and the Solar PV with the TS-PSS integrated respectively. The electromechanical modes showing the system eigenvalues is also shown in Table 4.10.

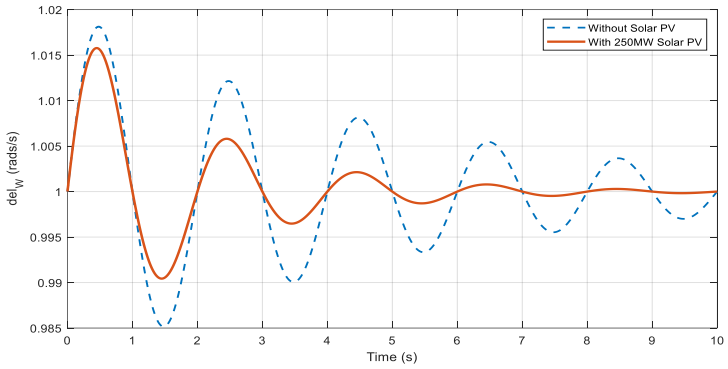

Figure 4.10 Generator rotor speed deviation in the SMIB with Solar PV Integrated

Table 4.10 System Eigenvalues before introduction of the TS-PSS

SMIB-PV Eigenvalues as a result of the fault	
Eigenvalues	**Damping Ratio**
0.4324 + 4.2603i	-0.2001
0.4324 – 4.2603i	-0.2001
-11.3120 + 0.0000i	1.000
-6.3220 + 0.0000i	1.000
-2.2531 + 0.0000i	1.000

TS-PSS is then implemented on the designed SMIB-PV-PSS system, Figure 4.11 shows the iteration curve of TS-PSS, which converged to its solution at iteration 22.

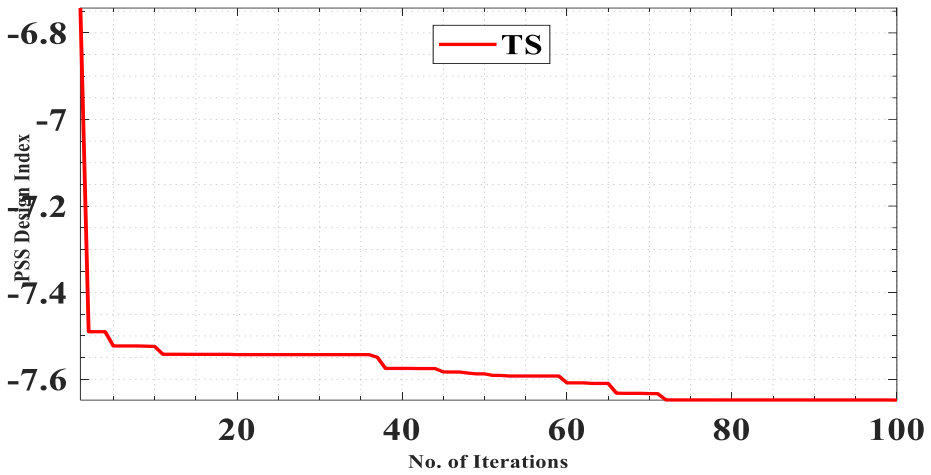

Figure 4.11 *Iteration curve of TS Algorithm*

The optimal PSS parameters obtained from the TS-PSS design are shown in Table 4.10. These parameters were used for simulation and the generator rotor speed deviation response to the simulation is shown in Figure 4.12.

Table 4.11 Showing the Optimal PSS parameters for the TS-PSS

Algorithm	Kpss	T1	T2	T3	T4
TS	99.9633	0.0689	0.6274	0.6422	0.0200

Also, the performance index from the simulation results above for TS-PSS in terms of rise and settling time for the generator rotor angle deviation is shown in Table 4.11

Table 4.12 SMIB-PV Settling & Rise Time

TS-PSS	SMIB -PV with TS-PSS	
	Settling Time (sec)	Rise Time (sec)
S_delta	3.0	0.35

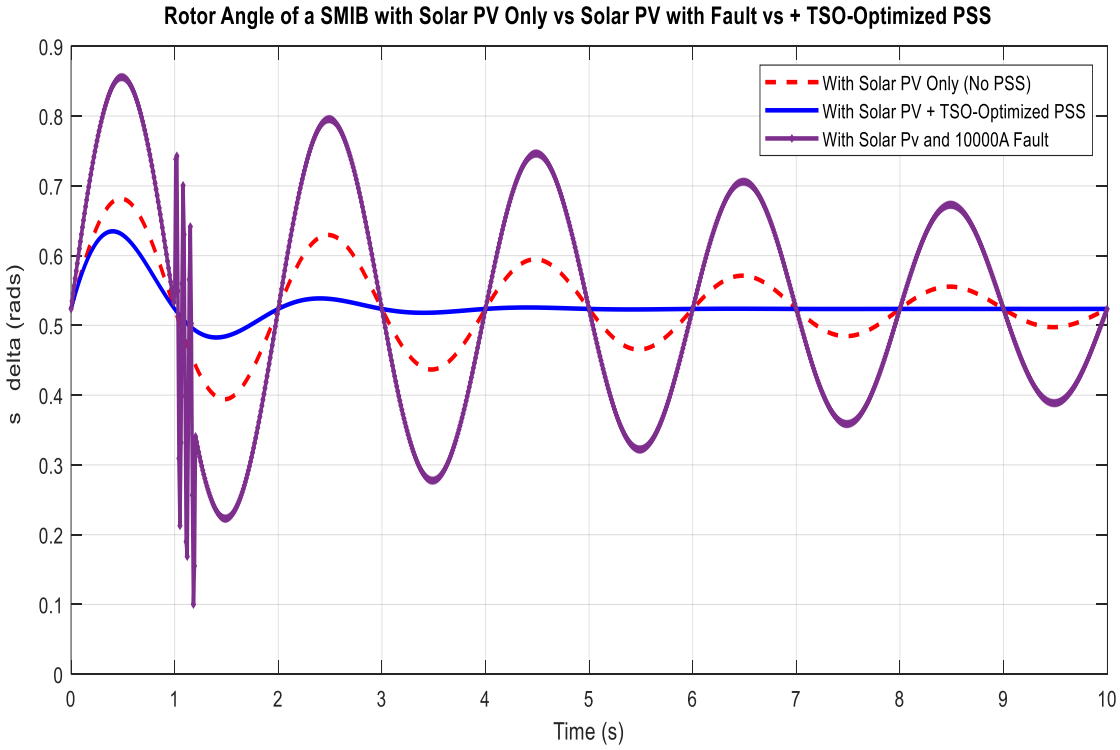

Figure 4.12 *SMIB_PV rotor angle deviation response to TS-PSS*

It can be seen from Table 4.12 that s_delta for the generator angle deviation for the TS-PSS controller in the system has a settling time of 3.0 seconds out of 10 seconds which is the simulation time. For the SMIB integrated with Solar PV system, Table 4.12 shows the dominant eigenvalues for the Electromechanical modes for TS-PSS and the corresponding damping ratio.

Table 4.13 SMIB-PV Eigenvalues and Damping Ratio of the TS Algorithm

Mode	SMIB-PV Eigenvalues as a result of the TS-PSS	Damping Ratio
1	61.2780 + 0.0000i	1.0000
2	-38.1768 +29.2432i	0.7939
3	-38.1768 -29.2432i	0.7939
4	-35.2345 + 0.0000i	1.0000
5	16.4414 + 0.0000i	-1.0000
6	-16.3824 + 0.0000i	1.0000
7	0.7289 + 0.0000i	-1.0000
8	-1.5599 + 0.0000i	1.0000
9	-0.0850 + 0.0000i	1.0000
10	-4.3780 + 0.0000i	1.0000
11	-4.9393 + 0.0000i	1.0000

5.1 Conclusion

The performance of the TS-PSS controller was then compared with established and frequently used algorithm such as the PSO and GA for PSS design using non-linear time domain simulation and quantitative analysis which is the second objective. The rotor speed and rotor angle were remarkably improved by the TS optimised PSS in terms of the settling time by an amount of 15.92% and 33.4% and 20.15 and 30% for the GA and PSO respectively and a 25% improvement for the rise time.

Furthermore, the PV solar energy system was integrated into the SMIB test model and a three phase balanced fault was also introduced to obtain the third objective of analysing the electromechanical modes as a result of introducing renewable energy to the power system. A robust TS-PSS damping controller was proposed in the integrated system.

Figure 4.12 illustrates the rotor angle deviation response of the SMIB system integrated with solar photovoltaic (PV) generation under three operating conditions: (i) solar PV without a power system stabilizer (PSS), (ii) solar PV with a TSO-optimized PSS, and (iii) solar PV subjected to a severe 10,000 A fault.

In the absence of a PSS, the system exhibits pronounced low-frequency oscillations with relatively large amplitude and slow decay. This behaviour indicates inadequate damping of electromechanical modes, which may compromise system stability under disturbances. The prolonged oscillatory response is reflected in a settling time of approximately 15.85s, demonstrating the limited effectiveness of the PV-integrated system without supplementary damping control.

With the introduction of the TSO-optimized PSS, a substantial improvement in dynamic performance is observed. The oscillation amplitude is significantly reduced, and the response converges more rapidly to its steady-state value. The optimized PSS effectively enhances the damping of the dominant electromechanical mode, resulting in smoother transient behaviour and improved system robustness. The settling time is reduced to approximately 3.0s, corresponding to a 81.0% improvement compared to the case without PSS. This reduction highlights the capability of the TSO-based optimization approach to fine-tune stabilizer parameters for superior dynamic response.

Under the severe fault condition, the system experiences large transient oscillations immediately following the disturbance, as expected. Although the oscillations gradually decay, the response remains significantly more oscillatory than in the optimized PSS case. This result emphasizes the importance of coordinated control strategies in PV-integrated power systems, particularly under high-impact disturbances.

Overall, the results confirm that the proposed TSO-optimized PSS markedly improves the small-signal and transient stability of the solar PV-integrated SMIB system. The observed reduction in settling time and oscillation magnitude demonstrates the effectiveness of the optimization framework in enhancing damping performance, thereby contributing to the reliable operation of power systems with high renewable energy penetration.

Key points to note are:

i. **Without PSS**, the synchronous generator already lacks damping for low-frequency electromechanical oscillations (~0.1–2 Hz).
ii. **Solar PV** systems do not contribute physical inertia or rotor damping, as they are power-electronics based.
iii. Thus, when a disturbance occurs (e.g., a fault or load change), oscillations in rotor angle may become more pronounced if no damping mechanism is added.

5.2 Contribution to the Body of Knowledge

i. Rotor angle stability analysis has been carried out on a single machine infinite bus system with the introduction of a balanced three-phase fault on the system, the generator rotor speed deviation response recorded a settling time of $3.04seconds$ and the generator rotor angle response a settling time of $3.10seconds$ out of 10seconds (simulation time). The introduction of the PSS damping controller using the TS algorithm improved the settling time of the generator rotor speed to $1.58seconds$ and that of the generator rotor angle to $1.32seconds$ which shows a remarkable 48% and 58% improvement respectively. The proposed PSS controller was validated by comparing it with PSO and GA PSS damping controllers to prove its robustness.

ii. In finding the optimal solution to the PSS design optimization problem for damping oscillations in the single-machine infinite bus system. TS converged fastest to the solution at the 20th iteration, PSO at 35, and GA at 30. The obtained PSS parameters were able to improve the dominant damping ratio of the single machine infinite bus system with no controller from 1.000 to 0.233 for TS-PSS, 0.4367 for GA-PSS, and 0.3286 for PSO-PSS

iii. The single-machine infinite bus system was then modified by incorporating a PV solar energy into the system. This introduced renewable energy source to the system. The introduction of the PV and the impact of a large three phase fault showed the effect on the system stability.

iv. TS-PSS damping controller was designed on the new system and the generator rotor angle deviation response in terms of settling time was recorded at 3.0secs out of 10 seconds (simulation time).

5.3 Recommendations

Based on the results obtained from the research work, the recommendations for future research are listed as follows:

i. Introduction of a conventional damper like the PSS inside the Inverter at the PV generator source. These dampers are called Power Oscillation dampers (PODs) and are similar to the traditional PSS dampers in function.
ii. Also, the introduction of controllers like flexible alternating current transmission systems (FACTS) with power oscillation damper (POD) can be introduced to the system.
iii. In addition, machine learning algorithms can be introduced in the optimal design of the damping controller.

REFERENCES

[1] R. Shah, N. Mithulananthan, R. C. Bansal, and V. K. Ramachandaramurthy, "A review of key power system stability challenges for large-scale PV integration," *Renew. Sustain. Energy Rev.*, vol. 41, pp. 1423–1436, 2015, doi: 10.1016/j.rser.2014.09.027.

[2] J. Rezaei, M. E. H. Golshan, and H. H. Alhelou, "Impacts of integration of very large-scale photovoltaic power plants on rotor angle and frequency stability of power system," *IET Renew. Power Gener.*, vol. 16, no. 11, pp. 2384–2401, 2022, doi: 10.1049/rpg2.12529.

[3] O. P. Veloza and F. Santamaria, "Analysis of major blackouts from 2003 to 2015: Classification of incidents and review of main causes," *Electr. J.*, vol. 29, no. 7, pp. 42–49, 2016, doi: 10.1016/j.tej.2016.08.006.

[4] S. Maity and R. Ramya, "A Comprehensive Review of Damping of Low Frequency Oscillations in Power Systems Low frequency oscillations, Robust power system Stabilizer View project," 2019. [Online]. Available: https://www.researchgate.net/publication/342393636

[5] A. Sabo, N. I. Abdul Wahab, M. L. Othman, M. Z. A. Mohd Jaffar, and H. Beiranvand, "Optimal design of power system stabilizer for multimachine power system using farmland fertility algorithm," *Int. Trans. Electr. Energy Syst.*, vol. 30, no. 12, pp. 1–33, 2020, doi: 10.1002/2050-7038.12657.

[6] B. Hoffschmidt *et al.*, "Concentrating solar power," *Compr. Renew. Energy*, vol. 3, no. 2, pp. 595–636, 2012, doi: 10.1016/B978-0-08-087872-0.00319-X.

[7] P. Kundur, *dokumen.tips_power-system-stability-and-control-by-prabha-kundur-577ff28fecd14*. 1994.

[8] P. Kundur *et al.*, "Definition and classification of power system stability," *IEEE Trans. Power Syst.*, vol. 19, no. 3, pp. 1387–1401, 2004, doi: 10.1109/TPWRS.2004.825981.

[9] M. A. Hannan *et al.*, "Artificial Intelligent Based Damping Controller Optimization for the Multi-Machine Power System: A Review," *IEEE Access*, vol. 6, pp. 39574–39594, Jul. 2018, doi: 10.1109/ACCESS.2018.2855681.

[10] N. Nikolaev, K. Dimitrov, and Y. Rangelov, "A comprehensive review of small-signal stability and power oscillation damping through photovoltaic inverters," *Energies*, vol. 14, no. 21, 2021, doi: 10.3390/en14217372.

[11] "Saadat - 1999 - Power System Analysis.pdf."

[12] A. Miller and B. Lumby, "Utility Scale Solar Power Plants," *Int. Financ. Corp. - World Bank Gr.*, pp. 1–204, 2012.

[13] P. Dey, A. Saha, A. Bhattacharya, and B. Marungsri, "Analysis of the Effects of PSS and Renewable Integration to an Inter-Area Power Network to Improve Small Signal Stability," *J. Electr. Eng. Technol.*, vol. 15, no. 5, pp. 2057–2077, 2020, doi: 10.1007/s42835-020-00499-2.

[14] M. December, "Solar Photovoltaic Power Plant Modeling and Validation Guideline Table of Contents," 2019.

[15] A. Nocoń and S. Paszek, "A Comprehensive Review of Power System Stabilizers," *Energies*, vol. 16, no. 4, 2023, doi: 10.3390/en16041945.

[16] A. Sabo *et al.*, "Farmland Fertility Optimization for Designing of Interconnected Multi-machine Power System Stabilizer," 2020. [Online]. Available: http://arqiipubl.com/ams

[17] A. H. Abd El-Kareem, M. Abd Elhameed, and M. M. Elkholy, "Effective damping of local low frequency oscillations in power systems integrated with bulk PV generation," *Prot. Control Mod. Power Syst.*, vol. 6, no. 1, Dec. 2021, doi: 10.1186/s41601-021-00219-6.

[18] S. M. Almufti, A. Ahmad Shaban, R. Ismael Ali, and J. A. Dela Fuente, "Overview of Metaheuristic Algorithms," *Polaris Glob. J. Sch. Res. Trends*, vol. 2, no. 2, pp. 10–32, Apr. 2023, doi: 10.58429/pgjsrt.v2n2a144.

[19] M. Mirrashid and H. Naderpour, "Transit search: An optimization algorithm based on exoplanet exploration," *Results Control Optim.*, vol. 7, no. January, p. 100127, 2022, doi: 10.1016/j.rico.2022.100127.

[20] P. W. Sauer, M. A. Pai, and J. H. Chow, *Power System Dynamics and Stability: With Synchrophasor Measurement and Power System Toolbox 2e*. 2017. doi: 10.1002/9781119355755.

[21] T. K. Renuka, P. Reji, and S. Sreedharan, "An enhanced particle swarm optimization algorithm for improving the renewable energy penetration and small signal stability in power system," *Renewables Wind. Water, Sol.*, vol. 5, no. 1, 2018, doi: 10.1186/s40807-018-0053-4.

[22] A. Sabo, T. E. Odoh, and N. I. A. Wahab, "Artificial Eco-System-Based Optimization Algorithm for Optimal Design of Single-Machine Infinite Bus and Multi-Machine Power System Stabilizers," *Electrica*, vol. 23, no. 3, pp. 522–533, Aug. 2023, doi: 10.5152/electrica.2023.22228.

[23] Y. L. Abdel-Magid and M. A. Abido, "Optimal multiobjective design of robust power system stabilizers using genetic algorithms," *IEEE Trans. Power Syst.*, vol. 18, no. 3, pp. 1125–1132, Aug. 2003, doi: 10.1109/TPWRS.2003.814848.

[24] A. Sabo, T. E. Odoh, H. Shahinzadeh, Z. Azimi, and M. Moazzami, "Implementing Optimization Techniques in PSS Design for Multi-Machine Smart Power Systems: A Comparative Study," *Energies*, vol. 16, no. 5, Mar. 2023, doi: 10.3390/en16052465.

[25] P. Dey, A. Bhattacharya, and P. Das, "Tuning of power system stabilizer for small signal stability improvement of interconnected power system," *Appl. Comput. Informatics*, vol. 16, no. 1–2, pp. 3–28, 2017, doi: 10.1016/j.aci.2017.12.004.

[26] D. U. Sarkar and T. Prakash, "A Recent Review on Approaches to Design Power System Stabilizers: Status, Challenges and Future Scope," 2023, *Institute of Electrical and Electronics Engineers Inc.* doi: 10.1109/ACCESS.2023.3244687.

[27] A. Sabo, N. I. A. Wahab, M. L. Othman, and M. Z. A. M. Jaffar, "Novel farmland fertility algorithm based pidpss design for smib angular stability enhancement," *Int. J. Adv. Sci. Technol.*, vol. 29, no. 6 Special Issue, pp. 873–882, 2020.

[28] N. Jankovic, J. Roldan-Perez, M. Prodanovic, J. A. Suul, S. D'Arco, and L. R. Rodriguez, "Power oscillation damping method suitable for network reconfigurations based on converter interfaced generation and combined use of active and reactive powers," *Int. J. Electr. Power Energy Syst.*, vol. 149, no. December 2022, p. 109010, 2023, doi: 10.1016/j.ijepes.2023.109010.

[29] B. Shao, Z. Miao, L. Wang, X. Meng, and Z. Chen, "ScienceDirect Low-frequency oscillation analysis of two-stage photovoltaic grid-connected system," *Energy Reports*, vol. 8, pp. 241–248, 2022, doi: 10.1016/j.egyr.2022.08.032.

[30] X. Zhang, C. Lu, S. Liu, and X. Wang, "A review on wide-area damping control to restrain inter-area low frequency oscillation for large-scale power systems with increasing renewable generation," *Renew. Sustain. Energy Rev.*, vol. 57, pp. 45–58, 2016, doi: 10.1016/j.rser.2015.12.167.

[31] G. N. Baltas, N. B. Lai, A. Tarraso, L. Marin, F. Blaabjerg, and P. Rodriguez, "AI-Based Damping of Electromechanical Oscillations by Using Grid-Connected Converter," *Front. Energy Res.*, vol. 9, no. March, pp. 1–17, 2021, doi: 10.3389/fenrg.2021.598436.

[32] Y. Shen, W. Yao, J. Wen, and H. He, "Adaptive wide-area power oscillation damper design for photovoltaic plant considering delay compensation," *IET Gener. Transm. Distrib.*, vol. 11, no. 18, pp. 4511–4519, 2017, doi: 10.1049/iet-gtd.2016.2057.

[33] P. Kabiru, K. Kaberere, and S. Kamau, "Design of a Robust Coordinated Power Oscillation Damper for Use with Large-Scale Wind Energy System Connected to a Multimachine Power System," *J. Electr. Comput. Eng.*, vol. 2022, 2022, doi: 10.1155/2022/5948356.

[34] A. Hoballah, "Impact of Large Penetration of Renewable Energy on Power System Transient Stability," in *22nd International Middle East Power Systems Conference, MEPCON 2021 - Proceedings*, IEEE, 2021, pp. 104–109. doi: 10.1109/MEPCON50283.2021.9686263.

[35] G. Parvathy and M. Sreekumar, "Website : www.ijareeie.com Analysis of Time Domain Specifications of a Large Scale PV Integrated Multi Machine Power System using LQR and LQG Control," pp. 2699–2707, 2017, doi: 10.15662/IJAREEIE.2017.0604086.

[36] R. Shah, N. Mithulananthan, and K. Y. Lee, "Large-scale PV plant with a robust controller considering power oscillation damping," *IEEE Trans. Energy Convers.*, vol. 28, no. 1, pp. 106–116, 2013, doi: 10.1109/TEC.2012.2230328.

[37] R. P. Schulz, *Synchronous Machine Modeling.*, no. 75 CHO970-4-PWR). 1975. doi: 10.1016/b978-0-12-811187-1.00003-2.

[38] L. Kunjumuhammed, S. Kuenzel, and B. Pal, "Case study of interarea oscillations in power system," *Simul. Power Syst. with Renewables*, pp. 1–15, 2020, doi: 10.1016/b978-0-12-811187-1.00008-1.

[39] L. Kunjumuhammed, S. Kuenzel, and B. Pal, "Modelling of solar generation," *Simul. Power Syst. with Renewables*, pp. 181–203, 2020, doi: 10.1016/b978-0-12-811187-1.00007-x.

[40] A. Sabo, N. I. A. Wahab, M. L. Othman, M. Z. A. M. Jaffar, H. Acikgoz, and H. Beiranvand, "Application of neuro-fuzzy controller to replace smib and interconnected multi-machine power system stabilizers," *Sustain.*, vol. 12, no. 22, pp. 1–42, Nov. 2020, doi: 10.3390/su12229591.

[41] C. Reeves, "Chapter 3 GENETIC ALGORITHMS Part A : Background," *Inf. Sci. (Ny).*, no. May, 1975, doi: 10.1007/978-1-4419-1665-5.

[42] A. Slowik, "Particle Swarm Optimization," *Ind. Electron. Handb. - Five Vol. Set*, no. December, 2011, doi: 10.1007/978-3-319-46173-1_2.